

Self-influenced growth through evolving material inhomogeneities

Original

Self-influenced growth through evolving material inhomogeneities / DI STEFANO, Salvatore; Ramírez-Torres, Ariel; Penta, Raimondo; Grillo, Alfio. - In: INTERNATIONAL JOURNAL OF NON-LINEAR MECHANICS. - ISSN 0020-7462. - 106:(2018), pp. 174-187. [10.1016/j.ijnonlinmec.2018.08.003]

Availability:

This version is available at: 11583/2720455 since: 2020-06-03T17:18:55Z

Publisher:

Elsevier Ltd

Published

DOI:10.1016/j.ijnonlinmec.2018.08.003

Terms of use:

This article is made available under terms and conditions as specified in the corresponding bibliographic description in the repository

Publisher copyright

Elsevier postprint/Author's Accepted Manuscript

© 2018. This manuscript version is made available under the CC-BY-NC-ND 4.0 license
<http://creativecommons.org/licenses/by-nc-nd/4.0/>. The final authenticated version is available online at:
<http://dx.doi.org/10.1016/j.ijnonlinmec.2018.08.003>

(Article begins on next page)

1 Self-influenced growth
2 through evolving material inhomogeneities

3 Salvatore Di Stefano^a, Ariel Ramírez-Torres^a,
4 Raimondo Penta^b, Alfio Grillo^{a,*}

5 ^a*Dipartimento di Scienze Matematiche (DISMA) “G.L. Lagrange”,*
6 *Politecnico di Torino, Corso Duca degli Abruzzi 24, 10129, Torino, Italy*
7 *E-mail: {salvatore.distefano ariel.ramirez alfio.grillo}@polito.it*

8 ^b*School of Mathematics and Statistics, Mathematics and Statistics Building,*
9 *University of Glasgow, University Place, Glasgow G12 8QQ, UK*
10 *E-mail: Raimondo.Penta@glasgow.ac.uk*

11 **Abstract**

We reformulate a model of avascular tumour growth in which the tumour tissue is studied as a biphasic medium featuring an interstitial fluid and a solid phase. The description of growth relies on two fundamental features: One of those is given by the mass transfer among the constituents of the phases, which is taken into account through source and sink terms; the other one is the multiplicative decomposition of the deformation gradient tensor of the solid phase, with the introduction of a *growth tensor*, which represents the growth-induced structural changes of the tumour. In general, such tensor is non-integrable, and it may allow to define a Levi-Civita connection with non-trivial curvature. Moreover, its evolution is related to the source and sink of mass of the solid phase through an evolution equation. Our goal is to study how growth can be influenced by the inhomogeneity of the growth tensor. To this end, we study the evolution of the latter, as predicted by two different models. In the first one, the dependence of the growth tensor on the tumour’s material points is not explicitly considered in the evolution equation. In the second model, instead, the inhomogeneity of the growth tensor is resolved explicitly by introducing the curvature associated with it into the evolution equation. Through numerical simulations, we compare the results produced by these two models, and we evaluate a possible role of the material inhomogeneities on growth.

12 *Keywords:* Growth, Remodelling, Material inhomogeneities, Inelastic
13 distortions

14 *2010 MSC:* 74Bxx, 74Cxx, 74Fxx, 76Sxx, 76Zxx, 92Bxx

[☆]Submitted to the Special Issue “Constitutive Modelling in Biomechanics”

*Corresponding author

Email address: alfio.grillo@polito.it (Alfio Grillo)

15 **1. Introduction**

16 Because of its repercussion on public health, the study of tumour growth is
17 a very active research field, to which mathematical modelling can give an im-
18 portant contribution [1, 2, 3]. A rather standard approach is to answer specific
19 questions at each scale of interest by formulating dedicated models. These can
20 be based on Statistical Mechanics [4], Kinetic Theories[5, 6, 7, 8, 9], and Con-
21 tinuum Mechanics [10, 11] (and references therein), depending on whether
22 the given problem involves the molecular, cellular, or the tissue scale. One of
23 the main challenges, however, is to understand the complexes of phenomena
24 that contribute to initiate the sprouting of a tumour, and to bridge across
25 the physical scales at which they occur. The difficulty arises, for instance,
26 when different types of models, conceived for different scales and disciplines,
27 have to be combined efficiently, and solved simultaneously.

28 Within the framework of Continuum Mechanics, the search for the multi-
29 scale and interdisciplinary approach outlined above is put into action by
30 formulating multiphasic, multi-scale models of tumour growth (see e.g. [12,
31 13, 14, 15, 16, 17]). In such models, growth is described as the mass variation
32 of the solid phase of the tumour at the expenses of its fluid constituents, and
33 the mass variation is often viewed as the result of the cooperation of both
34 chemical and mechanical factors [18].

35 From the point of view of Mechanics, a relevant aspect of growth is the
36 occurrence of structural transformations that accompany the “*visible*” mo-
37 tion of a tissue [19, 20] as well as its gain or loss of mass. All through the
38 years, a huge amount of literature has been produced on this subject, and
39 on the related issue of the residual stresses and strains that are expected to
40 exist in a grown material [21]. In fact, apart from [22] and some other recent
41 papers (see e.g. [23]), many works usually address the structural evolution of
42 a medium that grows or remodels by having recourse to the Bilby-Kröner-
43 Lee decomposition (BKL-decomposition) of the deformation gradient tensor
44 (see e.g. [10, 15, 19, 24, 25, 26, 27, 28, 29, 30, 31, 32, 33, 34, 35] and the
45 references therein). For a historically reliable review on the roots of the BKL
46 decomposition and on its significance in Differential Geometry, the Reader
47 is referred to [36] (Chapter 1, pp. 10–27) and to [37]. In both cases, the
48 Authors give due credit to the “old”, yet always up-to-date, ideas that have
49 led to what we nowadays know as BKL decomposition. In particular, the
50 review provided in [37] makes the uncommon effort of drawing the attention
51 of the Reader on some literature that, in spite of its importance, has not
52 become as popular as it deserved.

53 In the case of growth, the simplest version of the BKL-decomposition
54 consists of splitting the deformation gradient tensor of a tissue into an ac-

55 commodating factor and a growth factor (cf. Sect. 2). The latter one, denoted
 56 by \mathbf{F}_γ in the following, is often referred to as *growth tensor*, and is taken as
 57 the representative of the changes of the tissue’s internal structure.

58 The main properties of \mathbf{F}_γ are that it is non-integrable in general, and
 59 that it may induce a non-Euclidean metric tensor, $\mathbf{C}_\gamma = \mathbf{F}_\gamma^T \cdot \mathbf{F}_\gamma$. The latter
 60 can be employed to construct a Levi-Civita connection with a non vanishing
 61 fourth-order curvature tensor, \mathbf{R} . This result is consistent with the analysis
 62 of Kröner [38], according to whom the stress-free body pieces can be glued
 63 together in a non-Euclidean space. We emphasise that, in the context of
 64 growth, the concept of curvature has been explored e.g. in [39, 40, 41, 42,
 65 43, 44, 45] (see also [46]).

66 The introduction of the growth tensor, \mathbf{F}_γ , produces many similarities
 67 among growth, finite strain elastoplasticity, and the theory of defects in solids
 68 (see e.g. [47, 36] for a review) and, in fact, many biological aspects of growth
 69 can be re-interpreted in terms of the evolution of inelastic distortions. One
 70 similarity with elastoplasticity is the definition of a stress-free “intermediate
 71 configuration”, which exemplifies the conceptual separation between growth
 72 and deformation. Actually, the “intermediate configuration” is a collection of
 73 tissue pieces rather than a true configuration, and is obtained in two steps:
 74 First, by removing all the loads acting on the current configuration of the
 75 tissue, and then, by ideally chopping the tissue in small, stress-free pieces
 76 [36]. These can be assembled in a reference configuration by means of a
 77 transformation that is identifiable with \mathbf{F}_γ^{-1} . Hence, growth can be under-
 78 stood as the reverse process, which maps the tissue pieces from the reference
 79 configuration into the intermediate one.

80 Tensor \mathbf{F}_γ^{-1} is *formally* related to the existence of growth-induced in-
 81 homogeneities, [28, 42, 48, 49]. Note that we have emphasised the adverb
 82 “formally” because, in our theory, we are not using the concept of “*archetype*”
 83 [42, 48, 49]. This notion, instead, is used to define an inhomogeneous body
 84 as a body for which it is possible to define a non-singular tensor field, whose
 85 inverse is non-integrable [28, 42].

86 Clearly, the way in which the inhomogeneities evolve depends on the bio-
 87 logical problem under study and, thus, on the proposed model of growth. For
 88 instance, in [28], a prototypal evolution law for the growth inhomogeneities
 89 is set in the form of a relation between Eshelby stress and the rate at which
 90 the inhomogeneities themselves are produced. In this case, the evolution law
 91 is obtained by following a reduction procedure that requires its compliance
 92 with the body’s material symmetries, and with the principles of uniformity,
 93 objectivity, and independence of the reference configuration [28].

94 A different perspective is considered e.g. in [29, 50], where some phe-
 95 nomenological growth laws are discussed within a chemo-mechanical frame-

96 work. For arteries [51], an evolution law for the growth tensor is obtained
97 in terms of a generalised Onsager’s relation, in which the driving force of
98 growth is identified with the difference between a suitable measure of me-
99 chanical stress and a target stress, referred to as “*homeostatic stress*”.

100 As long as tumour growth is concerned, the hypothesis is often made
101 that the growth tensor is a pure dilatation [52, 53], thereby depending on one
102 parameter only, denoted by γ and referred to as “growth parameter” in the
103 sequel. In such cases, one has to supply an evolution law for γ (see e.g. (11b)
104 below), which translates the mass balance law for the tissue’s solid phase into
105 a kinematic constraint on γ itself [54, 55, 56, 57]. When this line of thought
106 is followed, the evolution of the growth tensor is entirely dictated by the law
107 describing the variation of mass of the tissue, denoted by r_s in our notation.

108 Since r_s is related to the rate of change of γ , the problem arises to de-
109 termine a generalised force that is conjugate to the variation of γ and that,
110 thus, triggers growth. However, since r_s is almost always assigned on the basis
111 of biological observations (see e.g. [55, 56]), which may be phenomenologi-
112 cal or “*micro-mechanically motivated*” [10], it may not be possible to identify
113 mechanical stress with the “driving force” that moves the growth-related dis-
114 tortions (i.e., the inhomogeneities, in the jargon of [28, 42]). This is, in fact,
115 a relevant difference with elastoplasticity, in general, and with the models
116 put forward in [28, 51], in which stress plays a central role. Indeed, it should
117 be emphasised that the growth of a tumour may occur also in the absence of
118 stress, whereas it strongly depends on the presence of nutrients, and may re-
119 sult in a loss of mass when these are unavailable. Still, stress may contribute
120 to modulate the way in which the mass change takes place [54, 58]. Perhaps,
121 we might say that, whereas stress is the “starring character” of pure remod-
122 elling (be it growth-induced or not), as it can be the trigger of the changes
123 of the tissue’s structure, it is somehow “downgraded” to a modulating factor
124 in the case of pure growth¹.

125 A rather different approach is suggested in [42], where the concept of “*self-*
126 *driven*” inhomogeneities is introduced. The underlying idea, framed within
127 the theory of defects in solids, could be rephrased as follows. Assume to have
128 an inhomogeneous solid medium with a non-uniform distribution of defects,
129 which can be modelled as incompatible distortions, and thus associated with
130 \mathbf{F}_γ . Assume, in addition, that the defects interact with each other, and that
131 the strength of their mutual interaction is accounted for by the variability of
132 \mathbf{F}_γ (i.e., the more \mathbf{F}_γ varies, the stronger the interaction is). Then, to adhere
133 to Epstein’s statement [42]:

¹We warmly thank Prof. Luigi Preziosi for several discussions on this issue.

134 “The evolution is intrinsic or self-driven if [...] the inhomogeneity
 135 moves just by virtue of its being there, perhaps in its effort to relax
 136 itself”

137 we claim that the spatial variability of \mathbf{F}_γ is sufficient to initiate a sponta-
 138 neous evolution of \mathbf{F}_γ in time.

139 In our work, we formulate a model of tumour growth based on the theo-
 140 ry presented in [42, 54]. We are interested in quantifying how, and to what
 141 extent, the inhomogeneities produced by growth influence the spatiotemporal
 142 evolution of γ . For this purpose, we propose a model that merges the
 143 quasi-phenomenological definition of r_s supplied in [54] with the concept of
 144 “self-driven” distortions put forward in [42]. The underlying idea is that the
 145 functional form of the source/sink of mass r_s should be modified by intro-
 146 ducing a term that takes explicitly into account the scalar curvature, κ_γ ,
 147 associated with \mathcal{R} (see Sect. 2.2). Our motivation for undertaking this task,
 148 inspired by [42], is to give a possible answer to the following question:

149 Let us “prepare” the tissue in some grown configuration, with
 150 initial distribution of γ , γ_{in} , corresponding to nonzero curvature,
 151 $\kappa_{\gamma_{\text{in}}}$. Then, giving for granted that growth produces inhomoge-
 152 neities [28, 42], what is the impact of the initial inhomogeneities
 153 on the growth of the tissue in the subsequent instants of time?

154 The remainder of this work is structured as follows: In Sect. 2, we provide
 155 the notation and the fundamental definitions used in our work. In Sect. 3,
 156 we formulate in detail our model of tumour growth. In Sect. 4, we solve a
 157 benchmark problem. In Sect. 5, we comment the results of our numerical
 158 simulations and, finally, in Sect. 6, we summarise our results, and outline
 159 some future research goals.

160 2. Theoretical background

161 2.1. Kinematics of growth

162 We indicate by \mathcal{B} a bounded region of the three-dimensional Euclidean
 163 space, \mathcal{S} , chosen as reference placement for the considered tissue. For every
 164 $X \in \mathcal{B}$ and every $x \in \mathcal{S}$, we introduce the tangent spaces $T_X\mathcal{B}$ and $T_x\mathcal{S}$ and
 165 the tangent bundles $T\mathcal{B} = \sqcup_{X \in \mathcal{B}} T_X\mathcal{B}$ and $T\mathcal{S} = \sqcup_{x \in \mathcal{S}} T_x\mathcal{S}$. Moreover, we
 166 denote by $\mathcal{B}(t) \equiv \chi(\mathcal{B}, t)$ the placement of the tissue at time $t \in \mathcal{I}$, where
 167 $\chi(\cdot, t) : \mathcal{B} \rightarrow \mathcal{S}$ is the *motion* and $\mathcal{I} \subset \mathbb{R}$ an interval of time. The tangent
 168 map $\mathbf{F}(\cdot, t) \equiv T\chi(\cdot, t)$ is the deformation gradient tensor, and is defined as
 169 $\mathbf{F}(\cdot, t) : T\mathcal{B} \rightarrow T\mathcal{S}$, so that, for every $X \in \mathcal{B}$, $\mathbf{F}(X, t)$ maps vectors of
 170 $T_X\mathcal{B}$ into vectors of $T_{\chi(X,t)}\mathcal{S}$, i.e., $\mathbf{F}(X, t) : T_X\mathcal{B} \rightarrow T_{\chi(X,t)}\mathcal{S}$.

171 **Remark 1.** *The “classical” definition of reference placement, or configura-*
172 *tion, although widely used in Solid Mechanics, may not apply to biological*
173 *tissues. To the best of our knowledge, this is particularly true for a medium*
174 *undergoing appositional growth, i.e., the process in which material particles*
175 *are either deposited on the growing medium, or depleted from it. In both cases,*
176 *the “number” of material particles constituting the medium varies with time*
177 *and, consequently, it is impossible to define a unique reference configuration*
178 *for the medium, at least in the classical sense [22]. Rather, as reported in*
179 *[22], “the reference configuration of a material point is defined at the time*
180 *it is deposited,” which means that, at different times, the medium has to*
181 *be associated with different reference configurations. In our setting, however,*
182 *we deal with volumetric growth. This type of growth, in fact, still permits*
183 *the definition of a fixed reference configuration for a growing medium if, as*
184 *stated in [28], the addition or depletion of material is assumed to occur “in*
185 *such a way that material points preserve their identity” . With the aid of this*
186 *hypothesis, we can assume the existence of a fixed reference configuration for*
187 *the medium under investigation.*

188 A major character of our theory is the BKL-decomposition, $\mathbf{F} = \mathbf{F}_e \mathbf{F}_\gamma$.
189 As anticipated in the Introduction, \mathbf{F}_γ describes the inelastic changes of
190 the tissue’s internal structure that are induced by growth, while \mathbf{F}_e is the
191 accommodating part of \mathbf{F} , and is assumed to be elastic. Both \mathbf{F}_e and \mathbf{F}_γ
192 are non-singular, and their determinants, $J_e = \det \mathbf{F}_e$ and $J_\gamma = \det \mathbf{F}_\gamma$, are
193 strictly positive.

194 For every pair $(X, t) \in \mathcal{B} \times \mathcal{I}$, we prescribe that $\mathbf{F}_\gamma(X, t)$ maps vectors of
195 $T_X \mathcal{B}$ into “relaxed” vectors of another tangent space. Such space is denoted
196 by $T_X \mathcal{N}_t$, and can be identified with the image of $T_X \mathcal{B}$ through $\mathbf{F}_\gamma(X, t)$
197 [45]. Coherently, we write $\mathbf{F}_\gamma(X, t) : T_X \mathcal{B} \rightarrow T_X \mathcal{N}_t$, and, putting together
198 this result and the definition of $\mathbf{F}(X, t)$, we express the elastic part of $\mathbf{F}(X, t)$
199 as $\mathbf{F}_e(X, t) : T_X \mathcal{N}_t \rightarrow T_{\chi(X, t)} \mathcal{S}$.

200 In general, the tissue may find itself in a stressed state both in the current
201 and in the reference configuration. Stresses may have different origin but, in
202 the present context, they are generated either by growth or by the loading
203 history undergone by the tissue. Since in our framework growth is the only
204 process regarded as inelastic, it produces stresses that cannot be eliminated
205 by simply switching off the applied loads. Indeed, even though all such loads
206 were suppressed, the tissue would still occupy a configuration in which the
207 growth-induced stresses are nonzero.

208 As mentioned in the Introduction, to achieve a state in which every part
209 of the tissue is free of stress, one should virtually disassemble the tissue into
210 a “conglomerate” of completely relaxed pieces [38]. Each of such pieces can

211 be thought of as an arbitrarily small neighbourhood of a point $x \in \mathcal{B}_t$, and,
 212 for infinitesimally small neighbourhoods, the body piece associated with x
 213 can be identified with the tangent space of \mathcal{B}_t at x , i.e., $T_x\mathcal{B}_t$. In this case,
 214 the whole relaxation can be viewed as a linear mapping between tangent
 215 spaces. In particular, since the relaxation is elastic, it is represented by
 216 $\mathbf{F}_e^{-1}(x, t) : T_x\mathcal{B}_t \rightarrow T_X\mathcal{N}_t$.

217 Although, $T_X\mathcal{N}_t$ is attached to the same point $X \in \mathcal{B}$ as $T_X\mathcal{B}$, it depends
 218 on time and, above all, it is associated with a state of the tissue characterised
 219 by an important property: it is free of stress, and is obtained by distorting
 220 the elements of $T_X\mathcal{B}$, or the elements of $T_x\mathcal{B}_t$, in a generally incompatible
 221 way. Hence, neither $\mathbf{F}_\gamma(X, t)$ nor $\mathbf{F}_e^{-1}(x, t)$ can be taken as the tangent maps
 222 of deformations evaluated at $X \in \mathcal{B}$ and $x \in \mathcal{B}_t$, respectively. Since this
 223 reasoning applies for each $X \in \mathcal{B}$, the tangent bundle $T\mathcal{N}_t = \sqcup_{X \in \mathcal{B}} T_X\mathcal{N}_t$
 224 cannot be associated with a configuration in the Euclidean space, and \mathcal{N}_t
 225 cannot be claimed to be a configuration in the classical sense. Rather, it
 226 is the *natural*, or ground, state of the tissue, i.e., the state in which the
 227 tissue is free of stress. Such state encompasses the whole structural evolution
 228 undergone by the tissue, which occurs from the reference configuration in the
 229 form of the distortional tensor map $\mathbf{F}_\gamma(\cdot, t) : T\mathcal{B} \rightarrow T\mathcal{N}_t$. A sketch of the
 230 explanation given so far is given in Fig. 1 (left), where \mathcal{N}_t is represented as
 231 a “conglomerate” of stress-free body pieces [38]. We recall, however, that \mathcal{N}_t
 232 can be assembled in a stress-free Riemannian manifold, endowed with the
 233 curved metric induced by \mathbf{F}_γ (cf. e.g. [38, 39, 45]).

234 We notice that, at this stage, \mathbf{F}_γ is not subjected to any restriction.
 235 Hence, granted the polar decompositions $\mathbf{F}_\gamma(X, t) = \mathbf{R}_\gamma(X, t)\mathbf{U}_\gamma(X, t)$ and
 236 $\mathbf{F}_\gamma(X, t) = \mathbf{V}_\gamma(X, t)\mathbf{R}_\gamma(X, t)$, which hold true for each pair $(X, t) \in \mathcal{B} \times \mathcal{I}$,
 237 $\mathbf{F}_\gamma(X, t)$ is generally obtained by combining one of the inelastic stretches,
 238 $\mathbf{U}_\gamma(X, t) : T_X\mathcal{B} \rightarrow T_X\mathcal{B}$ and $\mathbf{V}_\gamma(X, t) : T_X\mathcal{N}_t \rightarrow T_X\mathcal{N}_t$, with the rotation
 239 tensor $\mathbf{R}_\gamma(X, t) : T_X\mathcal{B} \rightarrow T_X\mathcal{N}_t$.

240 Before going further, we mention that a different formulation of the BKL-
 241 decomposition is presented in [59, 60]. The core of such formulation is the
 242 use of two mappings that define a base and a “target” [60] configuration for
 243 each of the factors of the BKL-decomposition. In summary, one indicates by
 244 \mathbf{F}_a and \mathbf{F}_g the accommodating and the growth part of \mathbf{F} , so that $\mathbf{F} = \mathbf{F}_a\mathbf{F}_g$
 245 holds true, and introduces the differentiable mappings χ_a and χ_g such that
 246 \mathbf{F}_a and \mathbf{F}_g are expressed as $\mathbf{F}_a = (T\chi_a)\mathbf{H}_a$ and $\mathbf{F}_g = (T\chi_g)\mathbf{H}_g$ [60]. Here,
 247 $T\chi_a$ and $T\chi_g$ are the tangent maps of χ_a and χ_g , and they represent the
 248 *compatible* contributions to \mathbf{F}_a and \mathbf{F}_g . On the contrary, in general \mathbf{H}_a and
 249 \mathbf{H}_g cannot be identified with the tangent map of any deformation. Indeed,
 250 \mathbf{H}_g describes the generally *incompatible* structural changes due to growth,
 251 while \mathbf{H}_a models the elastic distortions that may have to be applied to the

252 grown body pieces to restore a global configuration.

253 For every $t \in \mathcal{I}$, the map $\chi_g(\cdot, t)$ is identified with the diffeomorphism
 254 $\chi_g(\cdot, t) : \mathcal{B} \rightarrow \mathcal{C}_t$, where \mathcal{C}_t is referred to as “*intermediate configuration*”,
 255 while $T\chi_g(\cdot, t)$ and $\mathbf{H}_g(\cdot, t)$ are defined in terms of maps between tangent
 256 spaces, i.e., $T\chi_g(X, t) : T_X\mathcal{B} \rightarrow T_{\chi_g(X,t)}\mathcal{C}_t$ and $\mathbf{H}_g(X, t) : T_X\mathcal{B} \rightarrow T_X\mathcal{B}$,
 257 respectively [60]. Analogous considerations hold for $\chi_a(\cdot, t) : \mathcal{C}_t \rightarrow \mathcal{B}_t$ and
 258 for $T\chi_a(\cdot, t)$, and $\mathbf{H}_a(\cdot, t)$ (see [60] for details). A drawing summarising the
 259 view of the BKL-decomposition presented in [60] is given in Fig. 1 (right).
 260 We notice that \mathbf{H}_g plays the same role as \mathbf{F}_γ in the present context.

261 We emphasise that, although we do not use here the approach by [60],
 262 we find it important to draw attention on it because, through χ_g (or χ_a),
 263 it introduces an additional degree of freedom that, along with \mathbf{F}_γ , could be
 264 useful for other applications of the BKL-decomposition.

265 In the following, we investigate some consequences of the generally non-
 266 integrable nature of \mathbf{F}_γ on the evolution of growth itself (cf. also [39, 45]).

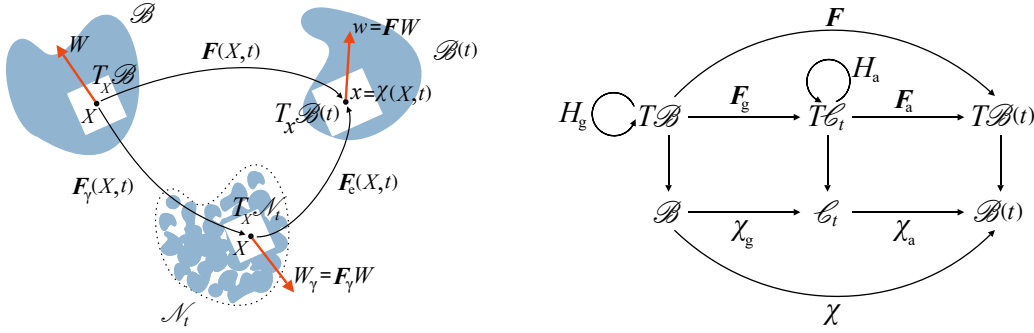


Figure 1: Schematic representation of the introduced mappings.

267 2.2. Growth and curvature

268 In this work, \mathbf{F}_γ is assumed to induce the Riemannian metric tensor

$$\mathbf{C}_\gamma = \mathbf{F}_\gamma^T \cdot \mathbf{F}_\gamma, \quad (1)$$

269 with is said to be the *growth metric tensor*. As pointed out in [59], \mathbf{C}_γ induces
 270 a Levi-Civita connection with non-trivial curvature [40, 41]. To see this, we
 271 first construct the Christoffel symbols of the connection, which, for a given
 272 coordinate system, are given by [61]

$$\Gamma_{MN}^A = \frac{1}{2} (\mathbf{C}_\gamma^{-1})^{AB} \left[\frac{\partial (\mathbf{C}_\gamma)_{BN}}{\partial X^M} + \frac{\partial (\mathbf{C}_\gamma)_{BM}}{\partial X^N} - \frac{\partial (\mathbf{C}_\gamma)_{MN}}{\partial X^B} \right], \quad (2)$$

273 and are symmetric in the lower indices, thereby implying the vanishing of
 274 the torsion [61], i.e.,

$$\mathbf{Tor} = (\Gamma_{MN}^A - \Gamma_{NM}^A) \mathbf{E}_A \otimes \mathbf{E}^M \otimes \mathbf{E}^N = \mathbf{0}. \quad (3)$$

275 Then, we compute the fourth-order curvature tensor generated by \mathbf{C}_γ , i.e.,
 276 $\mathcal{R} = \mathcal{R}^A_{BMN} \mathbf{E}_A \otimes \mathbf{E}^B \otimes \mathbf{E}^M \otimes \mathbf{E}^N$, whose components read [40, 41, 61]

$$\mathcal{R}^A_{BMN} = \frac{\partial \Gamma^A_{BN}}{\partial X^M} - \frac{\partial \Gamma^A_{BM}}{\partial X^N} + \Gamma^A_{MD} \Gamma^D_{BN} - \Gamma^A_{ND} \Gamma^D_{BM}. \quad (4)$$

277 Moreover, by contracting the first and the third index of \mathcal{R} , we obtain the
 278 Ricci curvature tensor,

$$\mathbf{R} = R_{BN} \mathbf{E}^B \otimes \mathbf{E}^N = \mathcal{R}^D_{BDN} \mathbf{E}^B \otimes \mathbf{E}^N, \quad (5)$$

279 and, by double-contracting \mathbf{R} with \mathbf{C}_γ^{-1} , we determine the scalar curvature
 280 associated with growth, i.e.,

$$\kappa_\gamma = \mathbf{R} : \mathbf{C}_\gamma^{-1}. \quad (6)$$

281 3. A model of tumour growth

282 We report on a mathematical model of tumour growth that, in spite of two
 283 important differences, largely follows the path designated in [54]. The first
 284 difference concerns the benchmark problem that we solve, whose geometry is
 285 much simpler than the one used therein. This choice is due to the fact that
 286 we are interested here in purely modelling issues. The second difference, as
 287 anticipated in Sect. 1, concerns the definition of the source/sink term r_s .

288 3.1. Growth and balance laws

289 By adhering to the model of tumour growth developed in [54], we describe
 290 a tumour in avascular stage as a biphasic medium comprising a solid and a
 291 fluid phase. At each point of the tissue, the amount of solid is measured by
 292 means of the apparent mass density $\varphi_s \varrho_s$, where φ_s and ϱ_s are said to be
 293 solid volumetric fraction and true mass density, respectively. Analogously,
 294 the amount of fluid is determined by the apparent density $\varphi_f \varrho_f$, with φ_f
 295 and ϱ_f being the volumetric fraction and true mass density, respectively. We
 296 recall that the *true* mass density of one of the phases constituting a mixture
 297 is the *intrinsic* mass density of the considered phase. In other words, it is
 298 the density that the phase would have if it were present in the mixture with
 299 unitary volumetric fraction. For this reason, the true mass density of a phase
 300 expresses its mass per unit volume of the phase itself, whereas the apparent

301 mass density expresses the phase mass per unit volume of the mixture as a
 302 whole.

303 Within our biphasic model, the tumour represents a saturated porous
 304 medium, so that the condition $\varphi_f = 1 - \varphi_s$ applies. Moreover, the fluid
 305 is assumed to feature only two constituents: nutrients, with mass fraction
 306 ω_N , and “water”, with mass fraction $\omega_w = 1 - \omega_N$. We hypothesise that ω_N
 307 is very small, so that the mass density of the fluid, ϱ_f , can be regarded as
 308 constant, and approximately equal to the mass density of water. What we
 309 call “water” here is, in fact, a fluid comprising several substances, among
 310 which the constituents of the dead cells that return to the fluid in order to
 311 be expelled.

312 For simplicity, we prescribe that the solid phase consists of two types
 313 of cells only: the proliferating cells, with mass fraction ω_p , and the necrotic
 314 cells, with mass fraction $\omega_n = 1 - \omega_p$. The former ones describe the gain of
 315 mass of the tissue in response to the consumption of the nutrients. However,
 316 they become necrotic when the nutrients fall below a given threshold. The
 317 necrotic cells, in turn, are absorbed by the fluid, thereby accounting for the
 318 tissue’s loss of mass due to cell death. In our model, the transition of a cell
 319 from the proliferating to the necrotic stage preserves the mass density of the
 320 cells. Hence, ϱ_s is independent of the composition of the solid phase, and
 321 may be regarded as constant, in spite of the fact that the mass fractions of
 322 the solid constituents may change in space and time [12, 54, 57].

323 To account for the gain and loss of mass pertaining to the proliferating
 324 and necrotic cells, we introduce their mass balance laws, which we write
 325 under the hypothesis that both types of cells move with the same velocity
 326 \mathbf{v}_s , i.e., the solid phase velocity. By extending the model developed in [54],
 327 we write such balance laws as

$$\partial_t(\varphi_s \varrho_s \omega_p) + \operatorname{div}(\varphi_s \varrho_s \omega_p \mathbf{v}_s) = r_{pn} + r_{fp} + r_{p\gamma}, \quad (7a)$$

$$\partial_t(\varphi_s \varrho_s \omega_n) + \operatorname{div}(\varphi_s \varrho_s \omega_n \mathbf{v}_s) = r_{np} + r_{nf} + r_{n\gamma}, \quad (7b)$$

328 where r_{pn} , r_{fp} , r_{np} , r_{nf} , $r_{p\gamma}$, and $r_{n\gamma}$ denote the rates of mass uptake or
 329 depletion for the solid constituents. In particular, r_{pn} describes the portion
 330 of proliferating cells that, per unit volume and unit time, is converted into
 331 necrotic cells. In turn, r_{np} is the rate at which the necrotic cells are generated
 332 at the expenses of the proliferating ones, so that the condition $r_{pn} + r_{np} = 0$
 333 is respected. Moreover, r_{fp} measures the growth of the proliferating cells
 334 due to the presence of nutrients, while r_{nf} represents the depletion of the
 335 necrotic cells in the fluid. We remark that r_{pn} , r_{fp} , r_{np} , and r_{nf} address
 336 processes that are at the basis of tumour evolution and, in this respect, their
 337 physical interpretation is rather intuitive. On the contrary, $r_{p\gamma}$ and $r_{n\gamma}$ are

338 introduced to investigate possible consequences of the properties of \mathbf{F}_γ on
 339 growth itself. In other words, their task is to establish a feed-back loop among
 340 growth, the distortions that it generates, i.e., \mathbf{F}_γ , and the influence of those
 341 on the mass exchange terms. To the best of our knowledge, the presence of
 342 $r_{p\gamma}$ and $r_{n\gamma}$ in (7a) and (7b) is a novelty in the framework of mathematical
 343 modelling of tumour growth.

344 Since the mass fraction of the necrotic cells can be written as $\omega_n = 1 - \omega_p$,
 345 Equation (7b) can be replaced by the mass balance law of the solid phase as
 346 a whole. Indeed, by adding together (7a) and (7b), we obtain [54]

$$\partial_t(\varphi_s \varrho_s \omega_p) + \operatorname{div}(\varphi_s \varrho_s \omega_p \mathbf{v}_s) = r_{pn} + r_{fp} + r_{p\gamma}, \quad (8a)$$

$$\partial_t(\varphi_s \varrho_s) + \operatorname{div}(\varphi_s \varrho_s \mathbf{v}_s) = r_s, \quad (8b)$$

347 where $r_s = r_{fp} + r_{nf} + r_{p\gamma} + r_{n\gamma}$ is the overall source/sink of mass for the solid
 348 phase. In general, this term can be diverted into changes either of density or
 349 of volume. In this work, since ϱ_s is constant, r_s is diverted into changes of
 350 volume. To show this, we perform the backward Piola transformation of (8a)
 351 and (8b) by multiplying both equations by $J = \det \mathbf{F}$. Then, by splitting J
 352 as $J = J_e J_\gamma$, with $J_e = \det \mathbf{F}_e$ and $J_\gamma = \det \mathbf{F}_\gamma$, we obtain

$$J_\gamma \Phi_{s\nu} \varrho_s \dot{\omega}_p = J[r_{pn} + r_{fp} + r_{p\gamma} - \omega_p r_s], \quad (9a)$$

$$\overline{(J_\gamma \Phi_{s\nu} \varrho_s)} = J r_s = J[r_{fp} + r_{nf} + r_{p\gamma} + r_{n\gamma}], \quad (9b)$$

353 where $\Phi_{s\nu} := J_e \varphi_s$ is the volumetric fraction of the solid phase expressed per
 354 unit volume of the intermediate, stress-free configuration. We require now
 355 that $\Phi_{s\nu}$ is constant in time. Since ϱ_s is constant too, the left-hand-side of
 356 (9b) is proportional to $\dot{J}_\gamma = J_\gamma \operatorname{tr}[\dot{\mathbf{F}}_\gamma \mathbf{F}_\gamma^{-1}]$. Hence, (9a) and (9b) become

$$\dot{\omega}_p = \frac{J[r_{pn} + r_{fp} + r_{p\gamma} - \omega_p r_s]}{J_\gamma \Phi_{s\nu} \varrho_s}, \quad (10a)$$

$$\operatorname{tr}[\dot{\mathbf{F}}_\gamma \mathbf{F}_\gamma^{-1}] = \frac{J[r_{fp} + r_{nf} + r_{p\gamma} + r_{n\gamma}]}{\Phi_{s\nu} \varrho_s J_\gamma}. \quad (10b)$$

357 In general, besides varying the mass of a tissue, growth may also induce
 358 isochoric distortions. Accordingly, \mathbf{F}_γ can be written as $\mathbf{F}_\gamma = [\det \mathbf{F}_\gamma]^{1/3} \bar{\mathbf{F}}_\gamma$,
 359 where $[\det \mathbf{F}_\gamma]^{1/3}$ measures the tissue's volume changes, and $\bar{\mathbf{F}}_\gamma$ is a volume-
 360 preserving tensor field that keeps track of the tissue's remodelling at constant
 361 mass. Thus, by adopting the notation $\gamma \equiv [\det \mathbf{F}_\gamma]^{1/3}$, we obtain [54]

$$\dot{\omega}_p = \frac{J[r_{pn} + r_{fp} + r_{p\gamma} - \omega_p r_s]}{J_\gamma \Phi_{s\nu} \varrho_s}, \quad (11a)$$

$$\frac{\dot{\gamma}}{\gamma} = \frac{J[r_{\text{fp}} + r_{\text{nf}} + r_{\text{p}\gamma} + r_{\text{n}\gamma}]}{3\Phi_{\text{sv}}\varrho_{\text{s}}J_{\gamma}}. \quad (11\text{b})$$

362 **Remark 2.** *The hypothesis of constant true mass density of the solid phase*
 363 *is due to the fact that such phase is considered to be a representation of*
 364 *the tissue's cells. These, in turn, are essentially made of water, whose mass*
 365 *density is constant in the biophysical range relevant to our work. It follows,*
 366 *thus, that also ϱ_{s} can be safely assumed to be constant. However, if this*
 367 *assumption is relaxed, Eq. (8b) can be recast in the form*

$$\overline{\dot{\varphi}_{\text{s}}\varrho_{\text{s}}} + \varphi_{\text{s}}\varrho_{\text{s}}\text{div}\mathbf{v}_{\text{s}} = r_{\text{s}}, \quad (12)$$

368 *and, by exploiting the identity $\dot{J} = J(\text{div}\mathbf{v}_{\text{s}})$, one can write*

$$J\dot{\varphi}_{\text{s}}\varrho_{\text{s}} + J\varphi_{\text{s}}\dot{\varrho}_{\text{s}} + \dot{J}\varphi_{\text{s}}\varrho_{\text{s}} = Jr_{\text{s}}. \quad (13)$$

369 *Since it holds that $\dot{J} = \dot{J}_{\text{e}}J_{\text{g}} + J_{\text{e}}\dot{J}_{\gamma} = J\text{tr}[\mathbf{L}_{\text{e}}] + J\text{tr}[\mathbf{L}_{\gamma}]$, with $\mathbf{L}_{\text{e}} = \dot{\mathbf{F}}_{\text{e}}\mathbf{F}_{\text{e}}^{-1}$*
 370 *and $\mathbf{L}_{\gamma} = \dot{\mathbf{F}}_{\gamma}\mathbf{F}_{\gamma}^{-1}$, one obtains*

$$J\dot{\varphi}_{\text{s}}\varrho_{\text{s}} + J\varphi_{\text{s}}\dot{\varrho}_{\text{s}} + J\varphi_{\text{s}}\varrho_{\text{s}}\text{tr}[\mathbf{L}_{\text{e}}] + J\varphi_{\text{s}}\varrho_{\text{s}}\text{tr}[\mathbf{L}_{\gamma}] = Jr_{\text{s}}. \quad (14)$$

371 *Moreover, we require $\text{tr}[\mathbf{L}_{\gamma}] = r_{\text{s}}/(\varphi_{\text{s}}\varrho_{\text{s}})$, so that (14) becomes*

$$\dot{\varphi}_{\text{s}}\varrho_{\text{s}} + \varphi_{\text{s}}\dot{\varrho}_{\text{s}} + \varphi_{\text{s}}\varrho_{\text{s}}\text{tr}[\mathbf{L}_{\text{e}}] = 0, \quad (15)$$

372 *which can be equivalently rearranged as $\overline{J_{\text{e}}\dot{\varphi}_{\text{s}}\varrho_{\text{s}}} = 0$. Thus, only the product*
 373 *$\varphi_{\text{s}}\varrho_{\text{s}}$, which individuates the mass density of the solid phase, is constant in*
 374 *time. Without loss of generality, it can be expressed with respect to the natural*
 375 *state, i.e., for $J_{\text{e}} = 1$, as*

$$J_{\text{e}}\varphi_{\text{s}}\varrho_{\text{s}} = \Phi_{\text{sv}}\varrho_{\text{s}0}, \quad (16)$$

376 *where Φ_{sv} is the volumetric fraction in the natural state, and $\varrho_{\text{s}0}$ denotes a*
 377 *constant reference value of the solid phase mass density. Equation (16) im-*
 378 *plies that $\varphi_{\text{s}}\varrho_{\text{s}}$ is a function of the elastic part of the overall deformation*
 379 *gradient tensor through J_{e} . In this case, ϱ_{s} can be either treated as an in-*
 380 *dependent variable of the theory or specified through a state law. If the first*
 381 *option is chosen, the model necessitates an additional equation determining*
 382 *the volumetric fraction (cf. e.g. [62, 63, 64]). If, instead, the second choice*
 383 *is made, and one assumes that ϱ_{s} is a constitutive function e.g. of the com-*

384 position of the solid phase, one obtains

$$\varphi_s = \frac{\Phi_{sv}\hat{\rho}_s(\omega_{p0})}{J_e\hat{\rho}_s(\omega_p)} = \frac{J_\gamma\Phi_{sv}\hat{\rho}_s(\omega_{p0})}{J\hat{\rho}_s(\omega_p)}. \quad (17)$$

385 Here, $\hat{\rho}_s(\omega_p)$ is the constitutive representation of the true mass density of the
 386 solid phase. As anticipated above, it is specified as a function of the com-
 387 position of the solid phase, which, within our model, is determined by the
 388 amount of proliferant and necrotic cells. Since it holds that $\omega_p + \omega_n = 1$, it
 389 suffices to use only one of the two mass fractions ω_p and ω_n to characterise
 390 the composition. Upon choosing ω_p , we let $\hat{\rho}_s$ depend on ω_p only, and we take
 391 ω_{p0} as a reference value for ω_p .

392 In conjunction with (11a) and (11b), also the mass balance laws of the
 393 nutrients and the fluid phase as a whole need to be studied

$$\partial_t(\varphi_f\varrho_f\omega_N) + \operatorname{div}(\varphi_f\varrho_f\omega_N\mathbf{v}_f + \mathbf{y}_N) = r_{Np}, \quad (18a)$$

$$\partial_t(\varphi_f\varrho_f) + \operatorname{div}(\varphi_f\varrho_f\mathbf{v}_f) = -r_s. \quad (18b)$$

394 In (18a) and (18b), \mathbf{v}_f is the velocity of the fluid, \mathbf{y}_N is the mass flux vector
 395 associated with the motion of the nutrients relative to the fluid phase, and r_{Np}
 396 is the rate at which the nutrients are “eaten” by the proliferating cells. We
 397 remark that, to ensure the conservation of the mass of the biphasic medium
 398 under study, the right-hand-side of (18b) is taken equal to the negative of r_s .

399 After some calculations, (18a) and (18b) can be rephrased as

$$\varphi_f\varrho_f\dot{\omega}_N + \varrho_f\mathbf{q}\operatorname{grad}\omega_N + \operatorname{div}\mathbf{y}_N = r_{Np} + \omega_N r_s, \quad (19a)$$

$$\operatorname{div}\mathbf{q} + \operatorname{div}\mathbf{v}_s = \left(\frac{1}{\varrho_s} - \frac{1}{\varrho_f}\right)r_s, \quad (19b)$$

400 where $\mathbf{q} = \varphi_f[\mathbf{v}_f - \mathbf{v}_s]$ is said to be filtration velocity. Finally, (19a) and (19b)
 401 can be pulled-back to the reference configuration, thereby obtaining

$$(J - J_g\Phi_{sv})\varrho_f\dot{\omega}_N + \varrho_f\mathbf{Q}\operatorname{Grad}\omega_N + \operatorname{Div}\mathbf{Y}_N = J[r_{Np} + \omega_N r_s], \quad (20a)$$

$$\operatorname{Div}\mathbf{Q} + \dot{j} = \left(\frac{1}{\varrho_s} - \frac{1}{\varrho_f}\right)Jr_s, \quad (20b)$$

402 where $\mathbf{Q} = J\mathbf{F}^{-1}\mathbf{q}$ is the material filtration velocity, and $\mathbf{Y}_N = J\mathbf{F}^{-1}\mathbf{y}_N$
 403 is the material mass flux vector of the nutrients. Under the hypothesis of
 404 validity of Darcy’s law for the fluid, and of Fick’s law for the nutrients, \mathbf{Q} and
 405 \mathbf{Y}_N read $\mathbf{Q} = -\mathbf{K}\operatorname{Grad}p$ and $\mathbf{Y}_N = -\varrho_f\mathbf{D}\operatorname{Grad}\omega_N$, with $\mathbf{K} = J\mathbf{F}^{-1}\mathbf{k}\mathbf{F}^{-T}$
 406 being the material permeability, p the pore pressure, and $\mathbf{D} = J\mathbf{F}^{-1}\mathbf{d}\mathbf{F}^{-T}$

407 the material diffusivity tensor of the nutrients in water. The tensors \mathbf{K} and
 408 \mathbf{D} are the backward Piola transforms of the spatial permeability, \mathbf{k} , and of
 409 the spatial diffusivity, \mathbf{d} , respectively.

410 To conclude, we introduce the momentum balance law for the biphasic
 411 medium as a whole, which we write directly in material form (see [54] for
 412 details), i.e.,

$$\text{Div} \left(-Jp \mathbf{g}^{-1} \mathbf{F}^{-\text{T}} + \mathbf{P}_{\text{sc}} \right) = \mathbf{0}, \quad (21)$$

413 where \mathbf{P}_{sc} is referred to as the constitutive part of the first Piola-Kirchhoff
 414 stress tensor of the solid phase.

415 3.2. Constitutive laws

416 In this work, the tumour tissue is assumed to be isotropic, and, for sim-
 417 plicity, \mathbf{k} and \mathbf{d} are taken “*unconditionally isotropic*” [65], which means that
 418 they are both proportional to the inverse metric tensor \mathbf{g}^{-1} . Hence, we write
 419 $\mathbf{k} = k_0 \mathbf{g}^{-1}$ and $\mathbf{d} = d_0 \mathbf{g}^{-1}$, where k_0 is given in the form of the Holmes-
 420 Mow scalar permeability [65, 66], and d_0 is defined as a function of J and J_γ
 421 through the fluid phase volumetric fraction, i.e.,

$$\begin{aligned} k_0 &= k_{\text{OR}} \left[\frac{\Phi_{\text{sv}} \varphi_{\text{f}}}{\varphi_{\text{f0}} \varphi_{\text{s}}} \right]^{m_0} \exp \left(\frac{m_1}{2} \left[\frac{J^2 - J_\gamma^2}{J_\gamma^2} \right] \right) \\ &= k_{\text{OR}} \left[\frac{J - J_\gamma \Phi_{\text{sv}}}{J_\gamma \varphi_{\text{f0}}} \right]^{m_0} \exp \left(\frac{m_1}{2} \left[\frac{J^2 - J_\gamma^2}{J_\gamma^2} \right] \right), \end{aligned} \quad (22a)$$

$$d_0 = \varphi_{\text{f}} d_{\text{OR}} = \frac{J - J_\gamma \Phi_{\text{sv}}}{J} d_{\text{OR}}. \quad (22b)$$

422 In (22a), $\varphi_{\text{f0}} = 1 - \Phi_{\text{sv}}$ is a reference value of the fluid phase volumetric frac-
 423 tion, m_0 and m_1 are constant material coefficients, and k_{OR} is said to be the
 424 reference permeability of the medium. This quantity is assumed to be a con-
 425 stant in this work, even though it should be defined as a function of material
 426 points in a more general setting. The factor d_{OR} in (22b) is the reference dif-
 427 fusivity, which, for simplicity, is assumed here to be constant. This condition,
 428 in fact, may be violated when the nutrient mass fraction, ω_{N} , is sufficiently
 429 greater than zero, in which case d_{OR} should be defined as a function of ω_{N} .

430 By substituting (22a) and (22b) into the definitions of \mathbf{k} and \mathbf{d} , and the
 431 corresponding results into the expressions of the material permeability and
 432 diffusivity, we find

$$\mathbf{K} = J k_0 \mathbf{C}^{-1}, \quad (23a)$$

$$\mathbf{D} = (J - J_\gamma \Phi_{\text{sv}}) d_{\text{OR}} \mathbf{C}^{-1}. \quad (23b)$$

433 Besides being isotropic, the solid phase of the tissue is assumed to be
 434 hyperelastic. Hence, its mechanical behaviour can be described by means of
 435 a strain energy density function, \mathcal{W} , which we express per unit volume of
 436 the reference configuration. To account for the variation of internal structure
 437 induced by growth, \mathcal{W} is given in terms of a constitutive function, $\tilde{\mathcal{W}}$, of \mathbf{F} ,
 438 \mathbf{F}_γ , and material points, X . The purely elastic contribution of the material
 439 to the overall energy can be measured by introducing the energy density \mathcal{W}_ν ,
 440 defined per unit volume of the stress-free configuration, whose associated
 441 constitutive representation, $\tilde{\mathcal{W}}_\nu$, depends on \mathbf{F} and \mathbf{F}_γ exclusively through
 442 \mathbf{F}_e . Hence, we write [28] (see also [67] for details)

$$\mathcal{W} = J_\gamma \mathcal{W}_\nu, \quad \tilde{\mathcal{W}}(\mathbf{F}, \mathbf{F}_\gamma, X) = J_\gamma \tilde{\mathcal{W}}_\nu(\mathbf{F}_e). \quad (24)$$

443 For $\tilde{\mathcal{W}}_\nu(\mathbf{F}_e)$, we choose a constitutive law of the Holmes-Mow type [66], i.e.,
 444

$$\begin{aligned} \tilde{\mathcal{W}}_\nu(\mathbf{F}_e) &= \hat{\mathcal{W}}_\nu(\mathbf{C}_e) = \check{\mathcal{W}}_\nu(\hat{I}_1(\mathbf{C}_e), \hat{I}_2(\mathbf{C}_e), \hat{I}_3(\mathbf{C}_e)) \\ &= \alpha_0 \left\{ \exp(\hat{\Psi}(\mathbf{C}_e)) - 1 \right\}, \end{aligned} \quad (25a)$$

$$\begin{aligned} \hat{\Psi}(\mathbf{C}_e) &= \check{\Psi}(\hat{I}_1(\mathbf{C}_e), \hat{I}_2(\mathbf{C}_e), \hat{I}_3(\mathbf{C}_e)) \\ &= \alpha_1 [\hat{I}_1(\mathbf{C}_e) - 3] + \alpha_2 [\hat{I}_2(\mathbf{C}_e) - 3] - \alpha_3 \ln(\hat{I}_3(\mathbf{C}_e)), \end{aligned} \quad (25b)$$

445 where $\mathbf{C}_e = \mathbf{F}_e^T \cdot \mathbf{F}_e$ is the elastic Cauchy-Green deformation tensor, $\hat{\mathcal{W}}_\nu(\mathbf{C}_e)$
 446 is introduced to comply with objectivity, and, to account for isotropy, the
 447 dependence of $\check{\mathcal{W}}_\nu$ on \mathbf{C}_e is expressed through the principal invariants

$$I_1 = \hat{I}_1(\mathbf{C}_e) = \text{tr}(\boldsymbol{\eta}^{-1} \mathbf{C}_e), \quad (26a)$$

$$I_2 = \hat{I}_2(\mathbf{C}_e) = \frac{1}{2} \{ [\hat{I}_1(\mathbf{C}_e)]^2 - \text{tr}[(\boldsymbol{\eta}^{-1} \mathbf{C}_e)^2] \}, \quad (26b)$$

$$I_3 = \hat{I}_3(\mathbf{C}_e) = \det \mathbf{C}_e. \quad (26c)$$

448 Here, $\boldsymbol{\eta}$ is the metric tensor of the “intermediate configuration” and, by using
 449 the equality $\mathbf{C}_e = \mathbf{F}_\gamma^{-T} \mathbf{C} \mathbf{F}_\gamma^{-1}$, it can be eliminated from (26a)–(26c), so that
 450 the invariants can be rephrased as functions of \mathbf{C} and \mathbf{C}_γ . Finally, in (25b),
 451 the material coefficients α_0 , α_1 , α_2 , and α_3 are functions of Lamé’s elastic
 452 parameters [68] (in particular, as in [66], we set $\alpha_3 = 1$), i.e.,

$$\alpha_0 = \frac{2\mu + \lambda}{4\alpha_3}, \quad \alpha_1 = \alpha_3 \frac{2\mu - \lambda}{2\mu + \lambda}, \quad \alpha_2 = \alpha_3 \frac{\lambda}{2\mu + \lambda}, \quad \alpha_3 = \alpha_1 + 2\alpha_2. \quad (27)$$

453 Equations (24), (25a), (25b), and (26a)–(26c) permit to calculate the consti-

454 tutive part of the second Piola-Kirchhoff stress tensor of the solid phase:

$$\begin{aligned} \mathbf{S}_{\text{sc}} &= \hat{\mathbf{S}}_{\text{sc}}(\mathbf{C}, \mathbf{C}_\gamma) = \left[J_\gamma \mathbf{F}_\gamma^{-1} \left(2 \frac{\partial \hat{\mathcal{W}}_\nu}{\partial \mathbf{C}_e}(\mathbf{C}_e) \right) \mathbf{F}_\gamma^{-\text{T}} \right] \\ &= 2J_\gamma b_1 \mathbf{C}_\gamma^{-1} + 2J_\gamma b_2 [I_1 \mathbf{C}_\gamma^{-1} - \mathbf{C}_\gamma^{-1} \mathbf{C} \mathbf{C}_\gamma^{-1}] + 2J_\gamma b_3 I_3 \mathbf{C}^{-1}, \end{aligned} \quad (28)$$

455 with $b_i = \partial \hat{\mathcal{W}}_\nu / \partial I_i$, $i \in \{1, 2, 3\}$. Consequently, the first Piola-Kirchhoff
456 stress tensor \mathbf{P}_{sc} can be expressed constitutively as

$$\mathbf{P}_{\text{sc}} = \hat{\mathbf{P}}_{\text{sc}}(\mathbf{F}, \mathbf{C}_\gamma) = \mathbf{F} \hat{\mathbf{S}}_{\text{sc}}(\mathbf{C}, \mathbf{C}_\gamma), \quad (29)$$

457 and, thus, the constitutive part of the Cauchy stress tensor reads

$$\begin{aligned} \boldsymbol{\sigma}_{\text{sc}} &= \hat{\boldsymbol{\sigma}}_{\text{sc}}(\mathbf{F}, \mathbf{C}_\gamma) = J^{-1} \hat{\mathbf{P}}_{\text{sc}}(\mathbf{F}, \mathbf{C}_\gamma) \mathbf{F}^{\text{T}} \\ &= \frac{J_\gamma}{J} \{ 2b_1 \mathbf{b}_e + 2b_2 [I_1 \mathbf{b}_e - \mathbf{b}_e \cdot \mathbf{b}_e] + 2b_3 I_3 \mathbf{g}^{-1} \}, \end{aligned} \quad (30)$$

458 where $\mathbf{b}_e = \mathbf{F} \mathbf{C}_\gamma^{-1} \mathbf{F}^{\text{T}}$ is the elastic right Cauchy-Green deformation tensor.

459 3.3. Sources and sinks of mass

460 To model growth, it is necessary to describe the mass exchanges among
461 the constituents of the system under study. In our framework, this requires
462 to provide mathematical expressions for r_{fp} , r_{pn} , r_{nf} , and r_{Np} , and to relate
463 each of these quantities with the appropriate set of chemo-mechanical vari-
464 ables. For r_{pn} , r_{nf} , r_{Np} and r_{fp} , we adopt the phenomenological expressions
465 suggested in [54], which we report here with slight changes of notation, i.e.,

$$r_{\text{pn}} = -\zeta_{\text{pn}} \left\langle 1 - \frac{\omega_{\text{N}}}{\omega_{\text{Ncr}}} \right\rangle_+ \varphi_{\text{s}} \omega_{\text{p}} = -\zeta_{\text{pn}} \left\langle 1 - \frac{\omega_{\text{N}}}{\omega_{\text{Ncr}}} \right\rangle_+ \frac{J_\gamma \Phi_{\text{sv}}}{J} \omega_{\text{p}}, \quad (31a)$$

$$r_{\text{nf}} = -\zeta_{\text{nf}} \varphi_{\text{s}} [1 - \omega_{\text{p}}] = -\zeta_{\text{nf}} \frac{J_\gamma \Phi_{\text{sv}}}{J} [1 - \omega_{\text{p}}], \quad (31b)$$

$$r_{\text{Np}} = -\zeta_{\text{Np}} \frac{\omega_{\text{N}}}{\omega_{\text{N}} + \omega_{\text{N0}}} \varphi_{\text{s}} \omega_{\text{p}} = -\zeta_{\text{Np}} \frac{\omega_{\text{N}}}{\omega_{\text{N}} + \omega_{\text{N0}}} \frac{J_\gamma \Phi_{\text{sv}}}{J} \omega_{\text{p}}, \quad (31c)$$

$$\begin{aligned} r_{\text{fp}} &= \zeta_{\text{fp}} \left\langle \frac{\omega_{\text{N}} - \omega_{\text{Ncr}}}{\omega_{\text{Nenv}} - \omega_{\text{Ncr}}} \right\rangle_+ \left[1 - \frac{\delta_1 \langle \bar{\sigma} \rangle_+}{\delta_2 + \langle \bar{\sigma} \rangle_+} \right] \frac{\varphi_{\text{f}} \varphi_{\text{s}}}{\varphi_{\text{f0}}} \omega_{\text{p}} \\ &= \zeta_{\text{fp}} \left\langle \frac{\omega_{\text{N}} - \omega_{\text{Ncr}}}{\omega_{\text{Nenv}} - \omega_{\text{Ncr}}} \right\rangle_+ \left[1 - \frac{\delta_1 \langle \bar{\sigma} \rangle_+}{\delta_2 + \langle \bar{\sigma} \rangle_+} \right] \frac{J - J_\gamma \Phi_{\text{sv}}}{J \varphi_{\text{f0}}} \frac{J_\gamma \Phi_{\text{sv}}}{J} \omega_{\text{p}}. \end{aligned} \quad (31d)$$

466 The terms r_{pn} , r_{nf} , and r_{Np} are sinks of mass for the constituents to which
467 they refer. In particular, r_{pn} represents the loss of mass of the proliferant
468 cells that become necrotic. The term r_{fp} , instead, is a source of mass for

469 the proliferant cells, and represents the mass gained by this population of
470 cells at the expenses of the fluid. We need to emphasise that both r_{pn} and r_{fp}
471 represent processes whose occurrence is strongly controlled by the availability
472 of the nutrients in the tissue. To describe mathematically the concept of
473 “availability of the nutrients”, we introduce a critical value of the nutrient
474 mass fraction, $\omega_{\text{Ncr}} \in]0, 1[$, and we model the transfers of mass associated
475 with r_{pn} and r_{fp} as threshold processes. Accordingly, when it holds that
476 $\omega_{\text{N}} \leq \omega_{\text{Ncr}}$, the proliferant cells die, which means that r_{pn} is active, while r_{fp}
477 is switched off. On the contrary, for $\omega_{\text{N}} > \omega_{\text{Ncr}}$, r_{pn} must vanish identically,
478 whereas r_{fp} is switched on. Such activation and deactivation of r_{pn} and r_{fp}
479 is formulated by means of the operator $\langle \cdot \rangle_+$, which returns the argument
480 to which it is applied, when the argument is greater than zero, and zero
481 otherwise. Thus, it is introduced to switch off cell death when the mass
482 fraction of the nutrients, ω_{N} , is above, or equal to, the threshold level $\omega_{\text{Ncr}} \in$
483 $]0, 1[$, which is assumed to be a constant of the model.

484 In our model, the coefficients ζ_{pn} , ζ_{nf} , ζ_{Np} and ζ_{fp} are constants, and
485 can be related to the characteristic time scales with which, respectively, the
486 proliferating cells die, the necrotic cells are converted into fluid, the nutrients
487 are consumed and the interstitial fluid becomes a tumor due to cell growth.

488 We notice that the sinks defined in (31a)–(31d) depend on the solid phase
489 volumetric fraction, $\varphi_{\text{s}} = (J_{\gamma} \Phi_{\text{sv}})/J$, in such a way that they vanish for
490 vanishing φ_{s} . For the same reason, r_{pn} must be zero for zero ω_{p} , r_{Np} must
491 be zero when ω_{p} or ω_{N} is zero, and r_{nf} must be zero for unitary ω_{p} , i.e.,
492 for zero ω_{n} (indeed, $\omega_{\text{n}} = 1 - \omega_{\text{p}}$). We remark, in addition, that the dependence
493 of r_{Np} on ω_{N} is taken from Population Dynamics [69], with the constant
494 $\omega_{\text{N0}} \in]0, 1[$ being a reference value of the nutrient concentration, introduced
495 to modulate the rate at which their uptake occurs. The dependence of r_{fp} on
496 φ_{s} and $\varphi_{\text{f}} = 1 - \varphi_{\text{s}}$ guarantees that growth ceases in the limit of compaction,
497 i.e., when all the fluid flows away, and the porous medium features no voids,
498 or when the solid disappears, which means that φ_{s} becomes zero. Besides,
499 r_{fp} vanishes for vanishing ω_{p} , and is modulated by stress through the term
500 $\langle \bar{\sigma} \rangle_+$, where $\bar{\sigma}$ is defined as

$$\bar{\sigma} = -\frac{1}{3}(\mathbf{g} : \boldsymbol{\sigma}_{\text{sc}}) = -\frac{\frac{2}{3} \sum_{i=1}^3 i b_i I_i}{J_{\text{e}}}. \quad (32)$$

501 We reserve now a separate treatment for the non-standard terms $r_{\text{p}\gamma}$ and
502 $r_{\text{n}\gamma}$. In particular, for the sake of simplicity, we set $r_{\text{n}\gamma} = 0$ and we prescribe
503 $r_{\text{p}\gamma}$ as

$$r_{\text{p}\gamma} = c \left[\zeta_{\text{fp}} \frac{\omega_{\text{N}}}{\omega_{\text{Ncr}}} \frac{\varphi_{\text{f}} \varphi_{\text{s}}}{\varphi_{\text{f0}}} \omega_{\text{p}} \right] \kappa_{\gamma} = c \left[\zeta_{\text{fp}} \frac{\omega_{\text{N}}}{\omega_{\text{Ncr}}} \frac{J - J_{\gamma} \Phi_{\text{sv}}}{J \varphi_{\text{f0}}} \frac{J_{\gamma} \Phi_{\text{sv}}}{J} \omega_{\text{p}} \right] \kappa_{\gamma}. \quad (33)$$

504 With the formulation of $r_{p\gamma}$ given in (33), we assume that $r_{p\gamma}$ is proportional
505 to κ_γ through the factor $c \zeta_{\text{fp}}(\omega_{\text{N}}/\omega_{\text{Ncr}})(\varphi_{\text{f}}\varrho_{\text{s}})/\varphi_{\text{f0}}$. In this work, the product
506 $c \zeta_{\text{fp}}$ is assumed to be constant and it represents, with respect to a suitable
507 time scale, the way in which the inhomogeneities induced by growth evolve
508 in the tissue. Moreover, as explained above for the standard terms (31a)–
509 (31d), we need to account for the limit cases in which compaction occurs
510 ($\varphi_{\text{f}} = 0$) or the solid phase is locally absent ($\varphi_{\text{s}} = 0$). In fact, we ensure
511 that $r_{p\gamma}$ vanishes when φ_{f} or φ_{s} vanish. Finally, we relate the availability of
512 nutrients to growth. In fact, we prescribe that growth does not take place if
513 $\omega_{\text{N}} = 0$, and we modulate the growth rate through the reference value ω_{Ncr} .
514 This factor, indeed, is introduced to re-scale the current mass fraction of the
515 nutrients, ω_{N} . In particular, the effect of κ_γ is amplified for $\omega_{\text{N}} > \omega_{\text{Ncr}}$, and
516 reduced for $\omega_{\text{N}} \leq \omega_{\text{Ncr}}$.

517 For the sake of a lighter exposition, in the present work we suppress the
518 rotations related to growth, so that \mathbf{R}_γ reduces to a shifter [61] from $T\mathcal{B}$
519 to $T\mathcal{N}_t$, and we assume that \mathbf{U}_γ represents a pure dilatation, i.e., we set
520 $\mathbf{U}_\gamma = \gamma\mathbf{I}$. This form of \mathbf{U}_γ also implies $J_\gamma = \gamma^3$ and $\mathbf{C}_\gamma = \gamma^2\mathbf{G}$, so that the
521 material metric, \mathbf{G} , is rescaled by γ^2 . Hence, no remodelling is considered in
522 this work, and growth is entirely expressed in terms of an evolution law for
523 γ , which, for given r_{fp} and r_{nf} , coincides with (11b).

524 We emphasise that the introduction of κ_γ in our model of tumour growth
525 is the major novelty of our work, and it constitutes the principal difference
526 with respect to the model developed in [54]. The difference is in the fact
527 that, while (11b) is an ordinary differential equation in [54], it is a partial
528 differential equation in our model. This feature of our approach allows for
529 an explicit resolution of the spatial variability of γ and, more importantly,
530 it permits to estimate to what extent such variability influences growth. In
531 fact, going through the calculations leading to (6), we notice that κ_γ features
532 the derivatives of γ up to the second order. Hence, by introducing $r_{p\gamma}$ into
533 (11b), we obtain a nonlinear diffusion-reaction like equation in the unknown
534 γ . Solving this equation shows how the resolved spatial variability of γ
535 influences the evolution of the other model descriptors, i.e., the mass fraction
536 of the proliferating cells, the mass fraction of the nutrients, the motion, and
537 pressure.

538 Looking at (11b), and combining it with the definitions (31b), (31d), and
539 (33), we notice that, when the mass fraction of the nutrients, ω_{N} , is below
540 the threshold ω_{Ncr} (so that $r_{\text{fp}} = 0$), we obtain

$$\frac{\dot{\gamma}}{\gamma} = c \left[\frac{\zeta_{\text{fp}}}{3\varrho_{\text{s}}} \frac{\omega_{\text{N}}}{\omega_{\text{Ncr}}} \frac{\varphi_{\text{f}}}{\varphi_{\text{f0}}} \omega_{\text{p}} \right] \kappa_\gamma - \frac{\zeta_{\text{nf}}}{3\varrho_{\text{s}}} [1 - \omega_{\text{p}}]. \quad (34)$$

541 In (34), indeed, the evolution of γ is governed by an affine function of κ_γ ,
 542 and is modulated by the mass fractions ω_p and ω_N . More generally, instead,
 543 when ω_N is above ω_{Ncr} , Equation (34) becomes:

$$\begin{aligned} \frac{\dot{\gamma}}{\gamma} = & c \left[\frac{\zeta_{fp}}{3\rho_s} \frac{\omega_N}{\omega_{Ncr}} \frac{\varphi_f}{\varphi_{f0}} \omega_p \right] \kappa_\gamma - \frac{\zeta_{nf}}{3\rho_s} [1 - \omega_p] \\ & + \frac{\zeta_{fp}}{3\rho_s} \left\langle \frac{\omega_N - \omega_{Ncr}}{\omega_{Nenv} - \omega_{Ncr}} \right\rangle_+ \left[1 - \frac{\delta_1 \langle \bar{\sigma} \rangle_+}{\delta_2 + \langle \bar{\sigma} \rangle_+} \right] \frac{\varphi_f}{\varphi_{f0}} \omega_p. \end{aligned} \quad (35)$$

544 Equation (35) combines two models: The first two terms on the right-hand-
 545 side of (35) are an adaptation of the model by Epstein [42] to our biphasic
 546 problem, which requires the introduction of the mass fraction of nutrients
 547 and proliferating cells as well as the volumetric fraction of the fluid phase.
 548 The last term, instead, is taken from the model by Mascheroni et al. [54] and
 549 has phenomenological nature in order to account for the fact that growth
 550 occurs when the mass fraction of the nutrients, ω_N , is greater than ω_{Ncr} , and
 551 it is modulated by stress.

552 **Remark 3.** *Following [42], one could formulate a more general model, with-*
 553 *out the a priori assumptions of no growth-induced rotations and $\mathbf{U}_\gamma = \gamma \mathbf{I}$.*
 554 *In this case, a possible evolution law for \mathbf{F}_γ could be obtained by relating $\dot{\mathbf{F}}_\gamma$*
 555 *to a known function of \mathcal{R} and $\text{Grad}\mathcal{R}$ [42]. Such an evolution law, however,*
 556 *is out of the scope of this work. Therefore, for the moment, we simply neglect*
 557 *$\text{Grad}\mathcal{R}$ in the evolution law for \mathbf{F}_γ , thereby keeping only its derivatives up to*
 558 *the second order. Moreover, since in our framework it holds that $\mathbf{U}_\gamma = \gamma \mathbf{I}$,*
 559 *we end up with model in which the evolution of γ is a function of the scalar*
 560 *curvature, κ_γ , whereas it does not depend on the spatial derivatives of γ of*
 561 *order higher than the second.*

562 4. Solution of a benchmark problem

563 4.1. Summary of the model

564 Before addressing the details of the considered benchmark problem, we
 565 summarise the model equations, and declare the unknowns to be determined.
 566 In doing this, we perform the following simplifications: (a) since the cells
 567 consist mainly of water, the mass densities ρ_s and ρ_f are regarded as equal
 568 to each other, so that the right-hand-side of (20a) is zero; (b) the advective
 569 term $\mathbf{Q} \text{Grad} \omega_N$ is considered to be negligible with respect to the other terms
 570 of (20a). In conclusion, the model equations are given by (11a), (11b), (20a),
 571 (20b), and (21), which we rewrite as

$$\text{Div} [-Jp\mathbf{g}^{-1} \mathbf{F}^{-T} + \mathbf{P}_{sc}] = \mathbf{0}, \quad (36a)$$

$$\dot{J} - \text{Div} [\mathbf{K} \text{Grad } p] = 0, \quad (36b)$$

$$(J - \gamma^3 \Phi_{sv}) \dot{\omega}_N - \text{Div} [\mathbf{D} \text{Grad } \omega_N] = J \left(\frac{r_{Np}}{\varrho_f} + \frac{3\gamma^3 \Phi_{sv} \omega_N \dot{\gamma}}{J \gamma} \right), \quad (36c)$$

$$\dot{\omega}_p = -\frac{\zeta_{pn}}{\varrho_s} \left\langle 1 - \frac{\omega_N}{\omega_{Ncr}} \right\rangle_+ \omega_p + \frac{\zeta_{nf}}{\varrho_s} [1 - \omega_p] + 3[1 - \omega_p] \frac{\dot{\gamma}}{\gamma}, \quad (36d)$$

$$\frac{\dot{\gamma}}{\gamma} = c \left[\frac{\zeta_{fp}}{3\varrho_s} \frac{\omega_N}{\omega_{Ncr}} \frac{J - \gamma^3 \Phi_{sv}}{J - J \Phi_{sv}} \omega_p \right] \kappa_\gamma + \frac{J[r_{fp} + r_{nf}]}{3\gamma^3 \Phi_{sv} \varrho_s}, \quad (36e)$$

572 where r_{nf} , r_{Np} , and r_{fp} are defined in (31b), (31c), and (31d). Consistently
 573 with (36a)–(36e), the unknowns of the models are the motion of the solid
 574 phase, χ , the pressure, p , the nutrient mass fraction, ω_N , the growth param-
 575 eter, γ , and the mass fraction of the proliferating cells, ω_p . Finally, \mathbf{K} , \mathbf{D} , and
 576 \mathbf{P}_{sc} are specified in (23a), (23b), and (29), and all the material parameters
 577 are reported in Table 1 and in Table 2.

578 4.2. Description of the benchmark test

579 As a proof of concept, we specialise now Equations (36a)–(36e) to a bench-
 580 mark problem taken from the literature. For our purposes, we select the
 581 problem of “*isotropic and homogeneous growth inside a rigid cylinder*”, for-
 582 mulated in [55] for the case of mono-phasic growing medium, and we adapt
 583 it to our scopes.

584 Also in our formulation, the growth is isotropic, i.e., $\mathbf{U}_\gamma = \gamma \mathbf{I}$, and takes
 585 place inside a tissue specimen of cylindrical shape, with undeformable curved
 586 surface. Hence, both the reference and the current configurations of the tissue
 587 have cylindrical shapes, with equal radius and different lengths. We indicate
 588 by R_{in} and L the initial radius and the initial length of the cylinder, re-
 589 spectively. Moreover, the reference configuration is covered with a system of
 590 cylindrical coordinates $\hat{X} = (R, \Theta, Z)$, where R , Θ , and Z are the radial,
 591 circumferential, and axial coordinate, respectively. Analogously, the generic
 592 current configuration of the tissue is covered with the system of cylindrical
 593 coordinates $\hat{x} = (r, \vartheta, z)$. Any rigid rotation of the specimen about the axis
 594 of the cylinder is suppressed from the outset.

595 The restrictions imposed on χ imply that only the axial component of
 596 the momentum balance law (36a) has to be solved, and that the sole un-
 597 known component of the motion is the axial one, χ^z , while the radial and
 598 circumferential ones, χ^r and χ^ϑ , return the radial and the angular coordinate,
 599 respectively.

600 The growth cannot be assumed to be homogeneous in our framework, as
 601 the scalar curvature, κ_γ , would then be trivially zero, and our model would
 602 boil down to a simple biphasic rephrasing of the model presented in [55]. On

603 the contrary, to highlight the role of κ_γ , we prescribe initial distributions of
 604 γ with a strong gradient.

605 In [55], the two extremities of the considered cylinder are free of applied
 606 forces, so that the axial component of stress is zero both at two outermost
 607 sections of the cylinder and, because of homogeneity, everywhere else in-
 608 side it. In our setting, however, we may only conclude that the overall axial
 609 Cauchy stress, $\sigma^{zz} = -p + \sigma_{sc}^{zz}$ is zero, whereas the pressure, p , and the
 610 constitutive Cauchy stress, σ_{sc}^{zz} , cannot be individually zero because of the
 611 point-dependent distribution of γ . In fact, they can be such only in the limit
 612 in which the initial inhomogeneities relax, and the conditions $p = 0$ and
 613 $\sigma_{sc}^{zz} = 0$ are the unique, stationary solutions to (36a) and (36b). Further
 614 differences with [55] are due to the different constitutive relations which we
 615 work with, and to the fact that our solid phase consists of two types of cells.

616 To solve (36a)–(36e) compatibly with the descriptions given so far, we
 617 prescribe the reference configuration of the tissue, \mathcal{B} , to be of cylindrical
 618 shape, and we assign the following set of boundary conditions, which apply
 619 for all times:

$$\chi^r = R_{\text{in}}, \quad \text{on } (\partial\mathcal{B})_{\text{C}}, \quad (37\text{a})$$

$$\chi^\vartheta = \Theta, \quad \text{on } (\partial\mathcal{B})_{\text{C}}, \quad (37\text{b})$$

$$(-Jp\mathbf{g}^{-1}\mathbf{F}^{-\text{T}} + \mathbf{P}_{\text{sc}}).\mathbf{N}_{\text{A}} = \mathbf{0}, \quad \text{on } (\partial\mathcal{B})_{\text{Left}} \text{ and } (\partial\mathcal{B})_{\text{Right}}, \quad (37\text{c})$$

$$(-\mathbf{K}\text{Grad}p).\mathbf{N}_{\text{C}} = 0, \quad \text{on } (\partial\mathcal{B})_{\text{C}}, \quad (37\text{d})$$

$$p = 0, \quad \text{on } (\partial\mathcal{B})_{\text{Left}} \text{ and } (\partial\mathcal{B})_{\text{Right}}, \quad (37\text{e})$$

$$(-\varrho_{\text{f}}\mathbf{D}\text{Grad}\omega_{\text{N}}).\mathbf{N}_{\text{C}} = 0, \quad \text{on } (\partial\mathcal{B})_{\text{C}}, \quad (37\text{f})$$

$$\omega_{\text{N}} = \omega_{\text{Nenv}}, \quad \text{on } (\partial\mathcal{B})_{\text{Left}} \text{ and } (\partial\mathcal{B})_{\text{Right}}, \quad (37\text{g})$$

$$(\text{Grad}\gamma)\mathbf{N} = 0, \quad \text{on } \partial\mathcal{B}. \quad (37\text{h})$$

620 In (37a)–(37g), $(\partial\mathcal{B})_{\text{C}}$ is the lateral boundary of the cylindric specimen,
 621 whereas $(\partial\mathcal{B})_{\text{Left}}$ and $(\partial\mathcal{B})_{\text{Right}}$ are the left and the right surfaces at the
 622 extremities of \mathcal{B} , respectively, \mathbf{N}_{A} is the unit vector field normal to $(\partial\mathcal{B})_{\text{Left}}$
 623 and $(\partial\mathcal{B})_{\text{Right}}$, \mathbf{N}_{C} is the unit vector field oriented normal to $(\partial\mathcal{B})_{\text{C}}$, and
 624 R_{in} is the initial radius of the cylinder. Furthermore, it holds that $\partial\mathcal{B} =$
 625 $(\partial\mathcal{B})_{\text{Left}} \cup (\partial\mathcal{B})_{\text{Right}} \cup (\partial\mathcal{B})_{\text{C}}$, and that \mathbf{N} is the unit vector field normal to
 626 $\partial\mathcal{B}$.

627 Before going further, we remark that the boundary conditions (37d) and
 628 (37f) describe the situation in which $(\partial\mathcal{B})_{\text{C}}$, besides being undeformable,
 629 is also impermeable to the fluid and to the nutrients. Finally, the Dirichlet
 630 condition (37g), with ω_{Nenv} kept constant in all calculations, means that the
 631 tissue specimen finds itself in a “bath” of nutrients, which can flow through
 632 the boundary surfaces $(\partial\mathcal{B})_{\text{Left}}$ and $(\partial\mathcal{B})_{\text{Right}}$.

633 Together with (37a)–(37g), we enforce the initial conditions:

$$\chi^r(R, \Theta, Z, 0) = R, \quad \chi^\vartheta(R, \Theta, Z, 0) = \Theta, \quad (38a)$$

$$\chi^z(R, \Theta, Z, 0) = Z + u_{\text{in}}(Z), \quad (38b)$$

$$p(R, \Theta, Z, 0) = 0, \quad (38c)$$

$$\omega_{\text{N}}(R, \Theta, Z, 0) = \omega_{\text{Nenv}}, \quad (38d)$$

$$\gamma(R, \Theta, Z, 0) = \gamma_{\text{in}}(Z), \quad (38e)$$

$$\omega_{\text{p}}(R, \Theta, Z, 0) = 1, \quad (38f)$$

634 which apply at all inner points of \mathcal{B} . The way in which the problem is
 635 formulated allows to infer that the deformation gradient tensor takes on
 636 the form $\mathbf{F} = \mathbf{e}_r \otimes \mathbf{E}^R + \mathbf{e}_\vartheta \otimes \mathbf{E}^\Theta + (1 + u')\mathbf{e}_z \otimes \mathbf{E}^Z$, where u is the axial
 637 displacement, the prime indicates partial differentiation in the axial direction
 638 (i.e., $u' \equiv \partial u / \partial Z$), while $\{\mathbf{e}_r, \mathbf{e}_\vartheta, \mathbf{e}_z\}$ and $\{\mathbf{E}^R, \mathbf{E}^\Theta, \mathbf{E}^Z\}$ are the vector basis
 639 and the co-vector basis generated by the coordinate systems $\hat{x} = (r, \vartheta, z)$ and
 640 $\hat{X} = (R, \Theta, Z)$, respectively. It is understood that $R \in [0, R_{\text{in}}]$, $\Theta \in [0, 2\pi[$,
 641 and $Z \in [-\frac{1}{2}L, \frac{1}{2}L]$.

642 As a further simplification, we require that all the physical quantities
 643 involved in the model are point-independent on each cross-section of the
 644 specimen, whereas they *do* vary along the axis of the cylinder, i.e., they are
 645 point-dependent only through the axial coordinate, Z . Therefore, the scalar
 646 curvature reads

$$\kappa_\gamma = \frac{2(\gamma')^2 - 4\gamma\gamma''}{\gamma^4} = \frac{6(\gamma')^2 - (4\gamma\gamma')'}{\gamma^4}, \quad (39)$$

647 and the model equations simplify as reported below:

$$[(\mathbf{P}_{\text{sc}})^{zZ}]' = p', \quad (40a)$$

$$\frac{\dot{\cdot}}{1 + u'} = \left[\frac{k_0}{1 + u'} p' \right]', \quad (40b)$$

$$\begin{aligned} [(1 + u') - \gamma^3 \Phi_{s\nu}] \dot{\omega}_{\text{N}} = & \left[\left(\frac{(1 + u') - \gamma^3 \Phi_{s\nu}}{(1 + u')^2} d_{0\text{R}} \right) \omega'_{\text{N}} \right]' \\ & + \gamma^3 \Phi_{s\nu} \left[3 \frac{\dot{\gamma}}{\gamma} \omega_{\text{N}} - \frac{\zeta_{\text{Np}}}{\varrho_{\text{f}}} \frac{\omega_{\text{N}}}{\omega_{\text{N}} + \omega_{\text{N0}}} \omega_{\text{p}} \right], \end{aligned} \quad (40c)$$

$$\dot{\omega}_{\text{p}} = -\frac{\zeta_{\text{pn}}}{\varrho_{\text{s}}} \left\langle 1 - \frac{\omega_{\text{N}}}{\omega_{\text{Ncr}}} \right\rangle_+ \omega_{\text{p}} + \frac{\zeta_{\text{nf}}}{\varrho_{\text{s}}} [1 - \omega_{\text{p}}] + 3[1 - \omega_{\text{p}}] \frac{\dot{\gamma}}{\gamma}, \quad (40d)$$

$$\frac{\dot{\gamma}}{\gamma} = |c| \left[\frac{\zeta_{\text{fp}}}{3\varrho_{\text{s}}} \frac{\omega_{\text{N}}}{\omega_{\text{Ncr}}} \frac{(1 + u') - \gamma^3 \Phi_{s\nu}}{(1 + u')(1 - \Phi_{s\nu})} \omega_{\text{p}} \right] \frac{4\gamma\gamma'' - 2(\gamma')^2}{\gamma^4}$$

$$\begin{aligned}
& + \frac{\zeta_{\text{fp}}}{3\rho_{\text{s}}} \left\langle \frac{\omega_{\text{N}} - \omega_{\text{Ncr}}}{\omega_{\text{Nenv}} - \omega_{\text{Ncr}}} \right\rangle_+ \left[1 - \frac{\delta_1 \langle \bar{\sigma} \rangle_+}{\delta_2 + \langle \bar{\sigma} \rangle_+} \right] \frac{(1 + u') - \gamma^3 \Phi_{\text{sv}}}{(1 + u')(1 - \Phi_{\text{sv}})} \omega_{\text{p}} \\
& - \frac{\zeta_{\text{nf}}}{3\rho_{\text{s}}} [1 - \omega_{\text{p}}], \tag{40e}
\end{aligned}$$

648 where we have set $J = 1 + u'$, and k_0 is defined in (22a). Equations (40a)–
649 (40d) are now put in weak form, and solved by employing the Finite Element
650 Method. To eliminate rigid motions along the axial direction, we introduce
651 a Dirichlet point for u at $Z = 0$, where we prescribe $u(0, t) = 0$ for all t .
652 Finally, we assign the initial conditions $\gamma_{\text{in}}(Z)$ and $u_{\text{in}}(Z)$ in such a way that
653 the problem results to be symmetric with respect to $Z = 0$.

Parameter	Unit	Value	Equation	Reference
L	[cm]	1.000	Initial length	—
R_{in}	[cm]	$1.000 \cdot 10^{-2}$	Initial radius	—
λ	[Pa]	$1.333 \cdot 10^4$	(27)	[70]
μ	[Pa]	$1.999 \cdot 10^4$	(27)	[70]
k_0	[mm ⁴ /(Ns)]	0.4875	(22a), (23a),	[66]
m_0	[–]	0.0848	(22a)	[66]
m_1	[–]	4.638	(22a)	[66]
$d_{0\text{R}}$	[m ² /s]	$3.200 \cdot 10^{-9}$	(22b), (40c)	[66]

Table 1: Parameters used in the definitions of the energy density, permeability and diffusivity. The mass fraction of the solid phase in the natural state is $\Phi_{\text{sv}} = 0.8$. The solid and fluid phase densities are $\rho_{\text{s}} = \rho_{\text{f}} = 1000 \text{ kg/m}^3$.

654 5. Results

655 To evaluate the impact of the scalar curvature, κ_{γ} , on the evolution of
656 the system under study, we solve (40a)–(40e) twice: First, we set $c = 0$ in
657 (40e), thereby switching off the term with κ_{γ} (this first model is denominated
658 M1). Then, we set $c \neq 0$, and solve (40a)–(40e), paying particular attention
659 to the effect of κ_{γ} (this second model is referred to as M2).

660 For our purposes, we prepare a protocol of numerical experiments in which
661 the initial distribution of the growth-related distortions, $\gamma_{\text{in}}(Z)$, has strong
662 gradients and non-vanishing curvatures. Specifically, we consider two types
663 of $\gamma_{\text{in}}(Z)$, i.e.,

$$\gamma_{\text{osc}}(Z) = f_0 + g_0 \cos(h_0 Z), \tag{41a}$$

$$\gamma_{\text{atan}}(Z) = \begin{cases} a_0 - b_0 \operatorname{atan}(r_0 (Z + \frac{1}{4}L)), & Z \in [-\frac{1}{2}L, 0], \\ a_0 + b_0 \operatorname{atan}(r_0 (Z - \frac{1}{4}L)), & Z \in]0, \frac{1}{2}L], \end{cases} \tag{41b}$$

Parameter	Unit	Value	Description	Reference
ζ_{fp}	[kg/(m ³ s)]	$1.343 \cdot 10^{-3}$	(31d),(33),(42)	[71]
ζ_{pn}	[kg/(m ³ s)]	$1.500 \cdot 10^{-3}$	(31a)	[71]
ζ_{nf}	[kg/(m ³ s)]	$1.150 \cdot 10^{-5}$	(31b)	[71]
ζ_{Np}	[kg/(m ³ s)]	$3.000 \cdot 10^{-4}$	(31c)	[72, 73]
c	[m ²]	$\{0, -10^{-6}\}$	(33)	—
g_0	[—]	$0.125 \cdot 10^{-1}$	(41a)	—
f_0	[—]	$1 + g_0$	(41a)	—
h_0	[1/cm]	8π	(41a)	—
a_0	[—]	1.020	(41b)	—
b_0	[—]	0.010	(41b)	—
r_0	[1/cm]	50π	(41b)	—
ω_{Ncr}	[—]	$1.000 \cdot 10^{-3}$	(31d), (33),(42)	—
ω_{Nenv}	[—]	$7.000 \cdot 10^{-3}$	(31d),(42)	—
ω_{N0}	[—]	$1.480 \cdot 10^{-4}$	(31c)	—
δ_1	[—]	$7.138 \cdot 10^{-1}$	(31d),(42)	[74]
δ_2	[Pa]	$1.541 \cdot 10^3$	(31d),(42)	[74]

Table 2: Parameters used in the definitions of the system’s geometry, in the definitions of the sources and sinks of mass, and in the initial conditions for γ .

664 both defining even functions with respect to $Z = 0$, and representing a grown
665 configuration of the tumour characterised by strong inhomogeneities. All the
666 parameters featuring in (41a) and (41b) are reported in Table 2. The models
667 ‘M1’ and ‘M2’ are further specialised in ‘M1(a)’ and ‘M2(a)’, for $\gamma_{\text{in}} = \gamma_{\text{osc}}$,
668 and ‘M1(b)’ and ‘M2(b)’, for $\gamma_{\text{in}} = \gamma_{\text{atan}}$.

669 5.1. Formulation of specialised sub-models

670 *Models M1(a) and M1(b) [no spatial resolution of the inhomogeneities].* We
671 solve (40a)–(40e) with $c = 0$, thereby switching off the curvature in the
672 simulations. Hence, (40e) reduces to the ordinary differential equation

$$\begin{aligned}
\frac{\dot{\gamma}}{\gamma} = & \frac{\zeta_{\text{fp}}}{3\rho_s} \left\langle \frac{\omega_{\text{N}} - \omega_{\text{Ncr}}}{\omega_{\text{Nenv}} - \omega_{\text{Ncr}}} \right\rangle_+ \left[1 - \frac{\delta_1 \langle \bar{\sigma} \rangle_+}{\delta_2 + \langle \bar{\sigma} \rangle_+} \right] \frac{(1 + u') - \gamma^3 \Phi_{s\nu}}{(1 + u')(1 - \Phi_{s\nu})} \omega_{\text{p}} \\
& - \frac{\zeta_{\text{nf}}}{3\rho_s} [1 - \omega_{\text{p}}], \tag{42}
\end{aligned}$$

673 and the boundary condition (37h) is no longer necessary. Therefore, together
674 with (40a)–(40d) and (42), only the boundary conditions (37a)–(37g) and the
675 initial conditions (38a)–(38f) have to be accounted for.

676 Although the spatial variability of γ does not play a direct role on (42),
677 the initial distribution of the growth-related distortions *does* influence the
678 evolution of γ .

679 *Models M2(a) and M2(b) [spatial resolution of the inhomogeneities].* We
 680 solve (40a)–(40e) with $c \neq 0$, and we enforce the complete set of bound-
 681 ary and initial conditions, i.e., (37a)–(37h) and (38a)–(38f), respectively. In
 682 this case, the scalar curvature, κ_γ , *does* contribute to drive the evolution of
 683 γ , through the first term on the right-hand-side of (40e).

684 5.2. Numerical results

685 In Fig. 2, we report the displacement of the tumour in the axial direction
 686 of the specimen, evaluated at the cross section of the cylinder $Z = L/2$, i.e.,
 687 $u(L/2, t) = \chi^z(L/2, t) - \chi^z(L/2, 0)$. As expected, in all the considered cases,
 688 the results of our simulations show that $u(L/2, t)$ increases monotonically
 689 with time. By comparing M1(a) with M2(a), and M1(b) with M2(b), we
 690 note that the curvature seems to play a significant role in the evolution of
 691 the tumour displacement. In fact, the inclusion of the curvature augments
 692 the steepness of the displacement from the beginning of the simulation, and,
 693 from the 3rd day onward, it increases its magnitude appreciably. This result
 694 suggests, in addition, that the initial curvature relaxes, and that the system,
 695 at the end of the simulation, finds itself in a less curved configuration. These
 696 deductions are confirmed by Fig. 3 and Fig. 4, in which the spatial distri-
 697 bution of the scalar curvature κ_γ , at the initial and final instants of time, is
 698 presented.

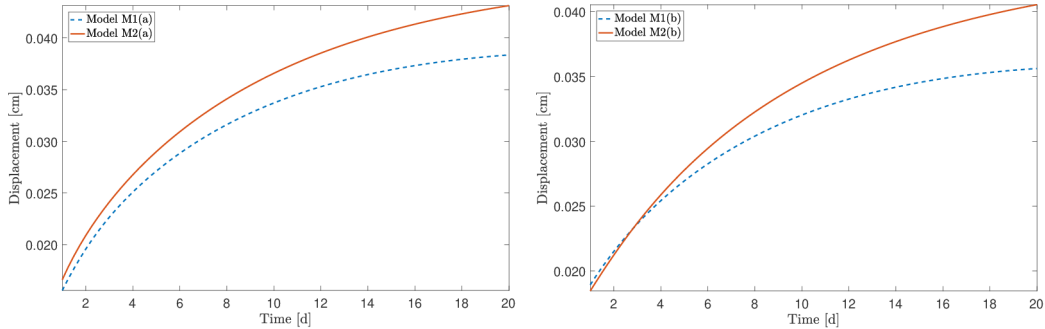


Figure 2: Evolution of the tumour in the axial direction, evaluated at the cross section $Z = L/2$. Panel on the left: comparison between M1(a) and M2(a), for which $\gamma_{\text{in}} = \gamma_{\text{osc}}$. Panel on the right: comparison between M1(b) and M2(b), for which $\gamma_{\text{in}} = \gamma_{\text{atan}}$.

699 Starting from Fig. 3, we note that the oscillating behaviour of the scalar
 700 curvature κ_γ , which reflects the trend of the initial distribution of the inho-
 701 mogeneities $\gamma_{\text{in}} = \gamma_{\text{osc}}$, results strongly mitigated at the end of the simulation.
 702 In fact, oscillations are appeased in this case, and κ_γ is closer to zero than
 703 the initial case, which means that tissue is evolving towards a configuration
 704 with reduced curvature. Analogously, in Fig. 4, the concentration of the gra-
 705 dient, which characterizes the scalar curvature for the model with $\gamma_{\text{in}} = \gamma_{\text{osc}}$,

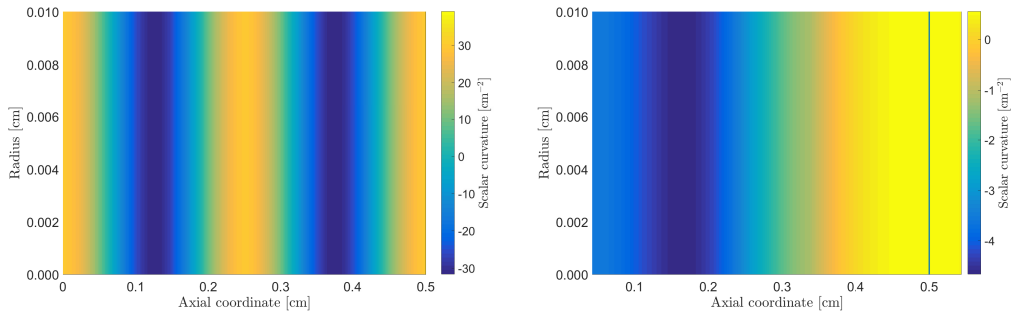


Figure 3: Spatial distribution of the scalar curvature κ_γ evaluated on the meridian section of the specimen, in the case of $\gamma_{\text{in}} = \gamma_{\text{osc}}$. Panel on the left: initial instant of time. Panel on the right: final instant of time.

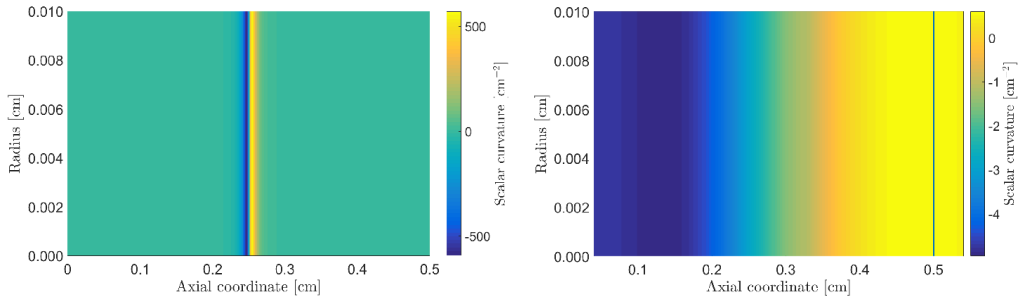


Figure 4: Spatial distribution of the scalar curvature κ_γ evaluated on the meridian section of the specimen, in the case of $\gamma_{\text{in}} = \gamma_{\text{atan}}$. Panel on the left: initial instant of time. Panel on the right: final instant of time.

706 relaxes at the end of the simulation. Also in this case, the tissue attains a fi-
 707 nal configuration in which the inhomogeneities are appreciably redistributed.
 708 The presence of the curvature κ_γ in the model and its relaxation, influences
 709 the spatial trend of the growth. In this sense, looking at Fig. 5, we notice
 710 that marked qualitative differences emerge among the spatial profiles of γ
 711 computed with M1(a) and M2(a), or M1(b) and M2(b). Still, if we neglect
 712 the embodiment of the curvature, the curves are qualitatively similar, with
 713 the magnitude increasing as time goes by. In particular, no peculiarity of
 714 the initial data seems to be found in the computed curves: The presence
 715 of oscillations in the case for which $\gamma_{\text{in}} = \gamma_{\text{osc}}$ (left), or the steep change in
 716 concavity, for the other choice of γ_{in} , i.e. $\gamma_{\text{in}} = \gamma_{\text{atan}}$ (right). On the other
 717 hand, when the curvature is explicitly considered, the spatial distribution
 718 of the growth is strongly influenced by the initial conditions. In detail, de-
 719 pending on time, the oscillations (left) and the rapid change in concavity
 720 (right), characterizing the two chosen initial distribution of inhomogeneities,
 721 are mitigated, but still present, until the end of the simulations. Although

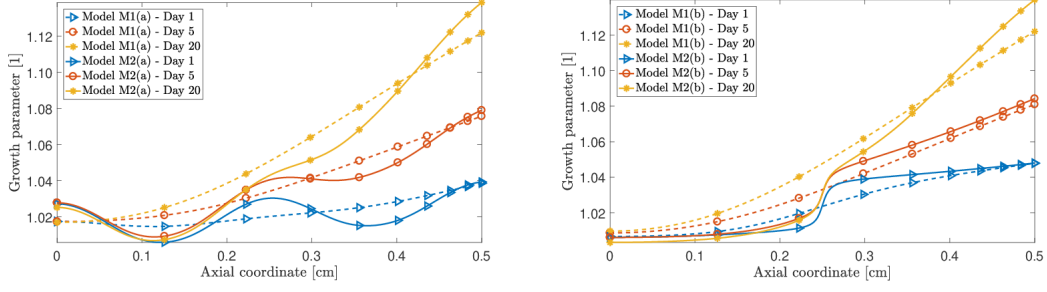


Figure 5: Spatial profile of the growth parameter γ for the models with $\gamma_{\text{in}} = \gamma_{\text{osc}}$ (panel on the left) and $\gamma_{\text{in}} = \gamma_{\text{atan}}$ (panel on the right). Since the problem is symmetric, only the half $[0, L/2]$ of the domain is shown.

722 the differences outlined above, and independently on the initial condition γ_{in} ,
 723 all the considered models lead to a final spatial behaviour of γ , in which the
 724 inhomogeneities are present.

725 Another point to put in evidence concerns Fig. 5 (left). The sub-system
 726 corresponding to the interval $[0, L/2]$ is initially symmetric with respect to
 727 $Z = L/4$. Yet, this further symmetry is lost in the course of time, as visible
 728 from the the spatial profile of γ . This peculiarity of the results could be ex-
 729 plained by referring to biological motivations, rather than geometric ones. To
 730 specify this aspect, let us focus on Fig. 6, which reports the trend of the nutri-
 731 ent mass fraction. We note, indeed, that the nutrients tend to diffuse from the
 732 boundaries $(\partial\mathcal{B})_{\text{Left}}$ and $(\partial\mathcal{B})_{\text{Right}}$ towards the centre of the specimen,
 733 along its axial direction. In the course of this process, there exists an instant
 734 of time after which the mass fraction of the nutrients becomes smaller than
 735 the critical value ω_{Ncr} in the interior of the tumour. Hence, while the growth
 736 of the tumour is inhibited in its centre, it is active close to the free bound-
 737 aries, where the mass fraction of the nutrients is still higher than the critical
 738 threshold.

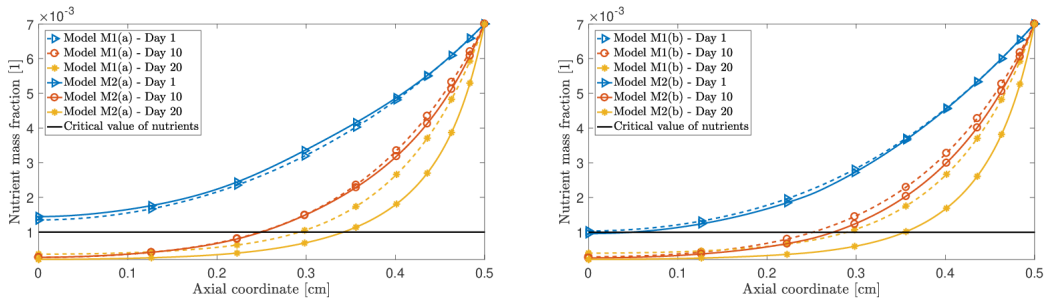


Figure 6: Spatial profile of the nutrient mass fraction ω_{N} for the models with $\gamma_{\text{in}} = \gamma_{\text{osc}}$ (panel on the left) and $\gamma_{\text{in}} = \gamma_{\text{atan}}$ (panel on the right). Since the problem is symmetric, only the half $[0, L/2]$ of the domain is shown.

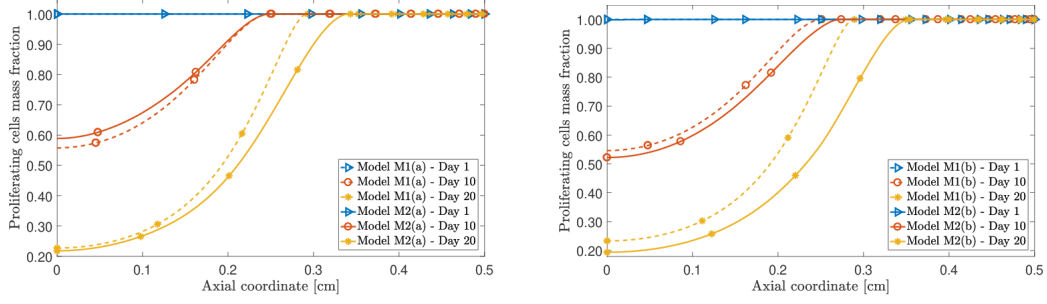


Figure 7: Spatial profile of the proliferating cells mass fraction ω_P for the models with $\gamma_{in} = \gamma_{osc}$ (panel on the left) and $\gamma_{in} = \gamma_{atan}$ (panel on the right). Since the problem is symmetric, only the half $[0, L/2]$ of the domain is shown.

739 A relevant result concerns the dynamics of the proliferating cells, as shown
 740 in Fig. 7. Their mass fraction, ω_P , remains close to unity in the proximity
 741 of the boundary $(\partial\mathcal{B})_{\text{Right}}$, where the level of nutrients is still high, while it
 742 diminishes in the centre of the tumour, where nutrients tend to become un-
 743 available (this means that the proliferating cells are “converted” into necrotic
 744 ones). This phenomenon is influenced by the explicit resolution of the cur-
 745 vature in the model. Indeed, when the curvature is explicitly considered, the
 746 conversion process of proliferating cells into necrotic ones is accelerated in
 747 the first days, and slowed down towards the end of the simulations. This
 748 behaviour occurs for both choices of γ_{in} , but appears to be slightly more
 749 pronounced for $\gamma_{in} = \gamma_{atan}$.

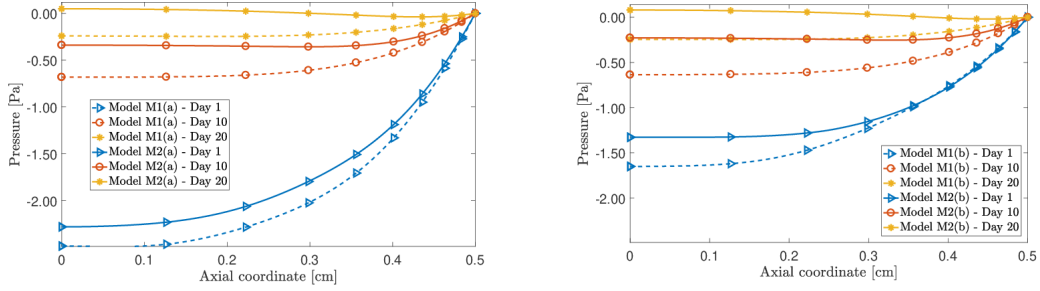


Figure 8: Spatial profile of the pore pressure p for the models with $\gamma_{in} = \gamma_{osc}$ (panel on the left) and $\gamma_{in} = \gamma_{atan}$ (panel on the right). Since the problem is symmetric, only the half $[0, L/2]$ of the domain is shown.

750 To proceed with our analysis, we refer to Fig. 8, where we plot the be-
 751 haviour of the pressure, p . When the tumour grows, the interstitial fluid flows
 752 towards the centre of the tumour, and p decreases from the free boundary
 753 (where the condition $p = 0$ applies) to the tumour’s interior, where it takes
 754 on negative values. However, when the system goes towards the end of the

755 simulations, p tends to become positive in the cases in which the curvature
 756 is explicitly accounted for, while it tends to zero from below otherwise.

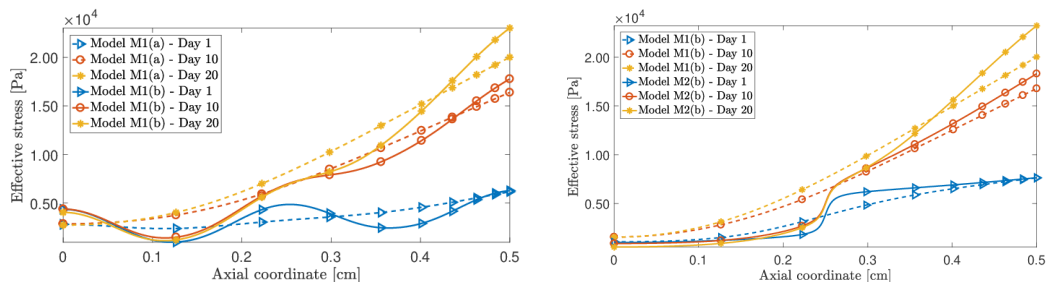


Figure 9: Spatial profile of the effective stress $\bar{\sigma}$ for the models with $\gamma_{\text{in}} = \gamma_{\text{osc}}$ (panel on the left) and $\gamma_{\text{in}} = \gamma_{\text{atan}}$ (panel on the right). Since the problem is symmetric, only the half $[0, L/2]$ of the domain is shown.

757 Finally, in Fig. 9, we display the effective stress $\bar{\sigma}$. First, we notice that
 758 the tumour is subjected to a compressive stress, since $\bar{\sigma}$ is positive. Apart
 759 from this result, which is common to all the studied cases, we report that the
 760 curvature modifies the qualitative behaviour of $\bar{\sigma}$. As final remark, we note
 761 how the spatial evolution of the stress in the specimen, independently of the
 762 model, is strongly affected by the initial distribution of the inhomogeneities.

763 6. Conclusion

764 In this work, a mathematical model addressing tumour growth has been
 765 presented. The mechanical framework has been developed by regarding the
 766 tumour as a multi-constituent, biphasic medium, and by enforcing the BKL-
 767 decomposition of the deformation gradient tensor. The growth of the tumour
 768 is influenced by both mechanical stimuli and biological factors, such as the
 769 nutrients transported by the interstitial fluid, and the interactions among
 770 proliferating and necrotic cells.

771 The principal novelty of our approach consists of a partial reformulation
 772 of the balance laws for the constituents of the solid phase, in such a way
 773 that it is introduced an explicitly dependence on the scalar curvature, κ_γ ,
 774 generated by the growth tensor $\mathbf{U}_\gamma = \gamma \mathbf{I}$ through the Riemannian, growth-
 775 related metric tensor $\mathbf{C}_\gamma = \gamma^2 \mathbf{G}$.

776 The introduction of κ_γ amounts to express the evolution law for γ as a
 777 partial differential equation, with the purpose of obtaining a better resolution
 778 of the material inhomogeneities, and an estimate of their influence on growth.
 779 To accomplish this task, we prescribe two types of initial conditions for γ ,
 780 both characterised by strong gradient and nonzero initial curvature, $\kappa_{\gamma_{\text{in}}}$.

781 Two more thoughts about our results may be worth to be mentioned.
782 The first one concerns the physical interpretation of the evolution of the
783 initial inhomogeneities accompanying γ_{in} . Indeed, since γ evolves according
784 to a generalised diffusion-reaction like equation, one may say that, in our
785 model, the material inhomogeneities brought about by growth “dissipate”
786 towards a configuration in which they are redistributed over the tissue. The
787 second thought pertains to the structure of the evolution equation (40e),
788 and is also related to the first one. Indeed, in the case in which the initial
789 inhomogeneities relax, the system tends to pass from a configuration in which
790 it is not invariant under material translations to a homogeneous configuration
791 in which it is translational invariant, thereby restoring the symmetry that is
792 initially broken by γ_{in} .

793 One limitation of our study is related to the fact that, in this work, we
794 have just relied on a phenomenological model in which κ_γ appears without a
795 strong theoretical justification. We have not built a systematic constitutive
796 framework, in which, for example, the strain energy density of our material
797 depends on γ *and* on κ_γ , nor have we conducted any study of the dissipation
798 inequality of the system at hand. Yet, confident in the intuitions that have
799 led to the model presented in [42], we hope that our results could provide a
800 basis for further investigations.

801 In our work, we concentrated on an academic benchmark problem in order
802 to compare our results with those of other Authors and, in particular, with
803 those of Ambrosi and Mollica [55]. For this reason, our general setting is *as*
804 simple *as* the setting of the problems taken as reference, expect for the fact
805 that we deal with a biphasic system featuring two cell populations and for the
806 fact that we account for the role of inhomogeneities through the introduction
807 of the term $r_{p\gamma}$ in the mass balance law of the proliferant cells. Clearly, our
808 model can be further generalised and, in our opinion, this could be done in
809 several steps. Here, we give some indications on how the formulation of our
810 problem should look like if such generalisations were done.

811 First, one could consider exactly the same framework and geometry as
812 the ones presented here, while relaxing the hypothesis of axial symmetry
813 of the problem. In this case, the initial inhomogeneities may vary not only
814 in the axial direction, but also radially or circumferentially, and the scalar
815 curvature κ_γ must be computed according to its own definition (6), since it
816 is no longer represented by (39). This requires the computation of all the
817 partial derivatives necessary to determine the Christoffel symbols as well as
818 the fourth-order curvature tensor specified in (4) and (5), respectively.

819 A second option could be to formulate an evolution law for γ in which the
820 evolution is driven by the full curvature tensor \mathcal{R} and its gradient $\text{Grad}\mathcal{R}$,
821 rather than by the scalar curvature only. In this case, the definitions of $r_{p\gamma}$

822 and $r_{n\gamma}$ should be further generalised, thereby implying a rewriting of the
823 mass balance laws of the proliferant and necrotic cells.

824 A further extension of the model could be the formulation of an evolution
825 law for the whole growth tensor \mathbf{F}_γ , with a restriction on $\text{tr}[\dot{\mathbf{F}}_\gamma \mathbf{F}_\gamma^{-1}]$, as done
826 in (10b). A model of this type extends the concept of growth presented in
827 this work and further rephrases the theory proposed in [42].

828 Another step is to specialise our model to problems with more realistic
829 geometries, which may arise from two- and three-dimensional studies. For a
830 given study, this means that the boundary value problem formulated in our
831 work has to be modified, and the Finite Element scheme adopted to solve it
832 has to be extended accordingly. In particular, the use of new computational
833 schemes may not be needed to resolve physical phenomena that could not be
834 captured otherwise, as is the case, for example, when the growth of a tumour
835 in the present of a host tissue and is studied [54].

836 Finally, although in the present work we dispensed with remodelling from
837 the outset, we are aware of the fact that such process accompanies growth.
838 In fact, it plays an important role in the redistribution of the mechanical
839 stress within the tissue and, thus, on the modulating effect of the latter
840 on the growth of a tumour. One possible way for studying remodelling is
841 to use the decompositions $\mathbf{F} = \mathbf{F}_e \mathbf{F}_r \mathbf{F}_\gamma$ or as $\mathbf{F} = \mathbf{F}_e \mathbf{F}_\gamma \mathbf{F}_r$, where \mathbf{F}_r
842 represents the distortion tensor describing the remodelling process, and to
843 study the dynamics of \mathbf{F}_r in relationship with all the other model variables. In
844 the literature, \mathbf{F}_r is often assumed to describe a plastic-like phenomenon
845 and is thus treated accordingly. Within the context of tumour growth, \mathbf{F}_r
846 accounts for the structural transformations of a tissue at the cellular level. Its
847 introduction requires to elaborate numerical schemes capable of capturing the
848 interplay between the growth and the structural evolution of a tissue, even
849 when these phenomena exhibit rather separated time scales.

850 Moreover, our model could be developed and extended to describe other
851 biological situations. For instance, the approach presented in this work for
852 isotropic media could be adapted for describing a tumour growing in anisotropic
853 tissues. Moreover, we could investigate the coupling with other remodelling
854 phenomena, introduced in term of cellular reorganisation, bluefibre reorienta-
855 tion or onset of degenerative phenomena. Finally, at the pore scale, the effect
856 of inhomogeneities could be studied by introducing a kinematic descriptor,
857 called “*intrinsic volume ratio*” [64].

858 Conflict of Interests

859 The Authors declare that they have no conflict of interests.

860 **Acknowledgments**

861 We thank Prof. Marcelo Epstein (The University of Calgary, Canada) for
862 proficuous discussions, which helped us in the understanding of his work.

863 **Article information**

864 DOI: 10.1016/j.ijnonlinmec.2018.08.003. Available online: August 10, 2018.
865 Journal: *International Journal of Non-Linear Mechanics* 106 (2018) 174-187

866 **References**

- 867 [1] R. P. Araujo, D. L. McElwain, A history of the study of solid tumour
868 growth: the contribution of mathematical modelling, *Bulletin of Math-*
869 *ematical Biology* doi:10.1016/s0092-8240(03)00126-5.
- 870 [2] T. Alarcón, H. Byrne, P. Maini, A cellular automaton model for tumour
871 growth in inhomogeneous environment, *Journal of Theoretical Biology*
872 225 (2) (2003) 257–274. doi:10.1016/s0022-5193(03)00244-3.
- 873 [3] G. W. Jones, S. J. Chapman, Modeling growth in biological materials,
874 *SIAM Review* 54 (1) (2012) 52–118. doi:10.1137/080731785.
- 875 [4] A. Guerra, D. Rodriguez, S. Montero, J. Betancourt-Mar, R. Martin,
876 E. Silva, M. Bizzarri, G. Cocho, R. Mansilla, J. Nieto-Villar, Phase tran-
877 sitions in tumor growth VI: Epithelial–mesenchymal transition, *Phys-*
878 *ica A: Statistical Mechanics and its Applications* 499 (2018) 208–215.
879 doi:10.1016/j.physa.2018.01.040.
- 880 [5] N. Bellomo, L. Preziosi, Modelling and mathematical problems re-
881 lated to tumor evolution and its interaction with the immune sys-
882 tem, *Mathematical and Computer Modelling* 32 (3-4) (2000) 413–452.
883 doi:10.1016/s0895-7177(00)00143-6.
- 884 [6] H. M. Byrne, M. A. Chaplain, Growth of nonnecrotic tumors in the
885 presence and absence of inhibitors., *Mathematical biosciences* 130 (1995)
886 151–181.
- 887 [7] H. Byrne, D. Drasdo, Individual-based and continuum models of growing
888 cell populations: a comparison, *Journal of Mathematical Biology* 58 (4-
889 5) (2009) 657–687. doi:10.1007/s00285-008-0212-0.

- 890 [8] P. Macklin, S. McDougall, A. R. A. Anderson, M. A. J. Chaplain,
891 V. Cristini, J. Lowengrub, Multiscale modelling and nonlinear simula-
892 tion of vascular tumour growth, *Journal of Mathematical Biology* 58 (4-
893 5) (2009) 765–798. doi:10.1007/s00285-008-0216-9.
- 894 [9] T. Roose, S. J. Chapman, P. K. Maini, Mathematical models of avascular
895 tumor growth, *SIAM Review* 49 (2) (2007) 179–208. doi:10.1137/
896 s0036144504446291.
- 897 [10] D. Ambrosi, G. Ateshian, E. Arruda, et al., Perspectives on biological
898 growth and remodeling, *J. Mech. Phys. Solids* 59(4) (2011) 863–883.
899 doi:10.1016/j.jmps.2010.12.011.
- 900 [11] J. D. Humphrey, Towards a theory of vascular growth and remodeling,
901 in: H. G.A., O. R.W. (Eds.), *Mechanics of Biological Tissue*, Springer-
902 Verlag, 2006, pp. 3–15. doi:10.1007/3-540-31184-x_1.
- 903 [12] H. Byrne, L. Preziosi, Modelling solid tumour growth using the theory
904 of mixtures, *Mathematical Medicine and Biology* 20 (4) (2003) 341–366.
905 doi:10.1093/imamb/20.4.341.
- 906 [13] L. Preziosi, G. Vitale, A multiphase model of tumor and tissue
907 growth including cell adhesion and plastic reorganization, *Math. Mod-
908 els Methods Appl. Sci.* 21 (09) (2011) 1901–1932. doi:10.1142/
909 s0218202511005593.
- 910 [14] D. Ambrosi, L. Preziosi, G. Vitale, The insight of mixtures theory for
911 growth and remodeling, *Z. Angew. Math. Phys.* 61 (2010) 177–191. doi:
912 10.1007/s00033-009-0037-8.
- 913 [15] A. Grillo, S. Federico, G. Wittum, Growth, mass transfer, and remodel-
914 ing in fiber-reinforced, multi-constituent materials, *Int. J. Nonlinear
915 Mech.* 47 (2012) 388–401. doi:10.1016/j.ijnonlinmec.2011.09.026.
- 916 [16] G. Ateshian, J. Humphrey, Continuum mixture models of biological
917 growth and remodeling: Past successes and future opportunities, *An-
918 nual Review of Biomedical Engineering* 14 (1) (2012) 97–111. doi:
919 10.1146/annurev-bioeng-071910-124726.
- 920 [17] R. D. O’Dea, S. L. Waters, H. M. Byrne, A multiphase model for tissue
921 construct growth in a perfusion bioreactor, *Mathematical Medicine and
922 Biology* 27 (2) (2010) 95–127. doi:10.1093/imamb/dqp003.

- 923 [18] D. Ambrosi, S. Pezzuto, D. Riccobelli, T. Stylianopoulos, P. Cia-
924 rletta, Solid tumors are poroelastic solids with a chemo-mechanical
925 feedback on growth, *J. Elast.* 129 (2017) 107–124. doi:10.1007/
926 s10659-016-9619-9.
- 927 [19] A. DiCarlo, S. Quiligotti, Growth and balance, *Mechanics Research*
928 *Communications* 29 (6) (2002) 449–456. doi:10.1016/s0093-6413(02)
929 00297-5.
- 930 [20] S. C. Cowin, G. A. Holzapfel, On the modeling of growth and adaptation,
931 in: H. G. A., O. R. W. (Eds.), *Mechanics of Biological Tissue*, Springer-
932 Verlag, 2006, pp. 29–46. doi:10.1007/3-540-31184-x_3.
- 933 [21] A. Guillou, R. W. Ogden, Growth in soft biological tissue and resid-
934 ual stress development, in: G. Holzapfel, R. Ogden (Eds.), *Mechanics*
935 *of Biological Tissue*, Springer-Verlag, 2006, pp. 47–62. doi:10.1007/
936 3-540-31184-x_4.
- 937 [22] G. A. Ateshian, On the theory of reactive mixtures for modeling biologi-
938 cal growth, *Biomechanics and Modeling in Mechanobiology* 6 (6) (2007)
939 423–445. doi:10.1007/s10237-006-0070-x.
- 940 [23] P. Ciarletta, M. Destrade, A. L. Gower, On residual stresses and home-
941 ostasis: an elastic theory of functional adaptation in living matter, *Sci-*
942 *entific Reports* 6 (1). doi:10.1038/srep24390.
- 943 [24] E. Kuhl, Growing matter: A review of growth in living systems, *J.*
944 *Mech. Behav. Biomed. Mater.* 29 (2014) 529–543. doi:10.1016/j.
945 jmbbm.2013.10.009.
- 946 [25] J. D. Humphrey, K. R. Rajagopal, A constrained mixture model
947 for growth and remodeling of soft tissues, *Mathematical Models and*
948 *Methods in Applied Sciences* 12 (03) (2002) 407–430. doi:10.1142/
949 s0218202502001714.
- 950 [26] E. Rodriguez, A. Hoger, A. McCulloch, Stress-dependent finite growth
951 in soft elastic tissues, *J. Biomech.* 27 (1994) 455–467. doi:https://
952 doi.org/10.1016/0021-9290(94)90021-3.
- 953 [27] L. A. Taber, Biomechanics of growth, remodeling, and morphogene-
954 sis, *Applied Mechanics Reviews* 48 (8) (1995) 487. doi:10.1115/1.
955 3005109.

- 956 [28] M. Epstein, G. A. Maugin, Thermomechanics of volumetric growth in
957 uniform bodies, *International Journal of Plasticity* 16 (7-8) (2000) 951–
958 978. doi:10.1016/s0749-6419(99)00081-9.
- 959 [29] K. Garikipati, E. Arruda, K. Grosh, H. Narayanan, S. Calve, A con-
960 tinuum treatment of growth in biological tissue: the coupling of mass
961 transport and mechanics, *J. Mech. Phys. Solids* 52 (2004) 1595–1625.
962 doi:10.1016/j.jmps.2004.01.004.
- 963 [30] B. Loret, F.M.F. Simões, A framework for deformation, generalized
964 diffusion, mass transfer and growth in multi-species multi-phase bio-
965 logical tissues, *Eur. J. Mech. A* 24 (2005) 757–781. doi:10.1016/j.
966 euromechsol.2005.05.005.
- 967 [31] R. K. Jain, J. D. Martin, T. Stylianopoulos, The role of mechanical
968 forces in tumor growth and therapy, *Annu. Rev. Biomed. Eng.* 16 (2014)
969 321–346. doi:10.1146/annurev-bioeng-071813-105259.
- 970 [32] M. Böl, A. B. Albero, On a new model for inhomogeneous volume growth
971 of elastic bodies, *J. Mech. Beh. Biom. Mat.* 29 (2014) 582–593. doi:
972 10.1016/j.jmbbm.2013.01.027.
- 973 [33] A. Ramírez-Torres, R. Rodríguez-Ramos, J. Merodio, J. Bravo-
974 Castellero, R. Guinovart-Díaz, J. Alfonso, Mathematical modeling of
975 anisotropic avascular tumor growth, *Mechanics Research Communica-*
976 *tions* 69 (2015) 8–14. doi:10.1016/j.mechrescom.2015.06.002.
- 977 [34] A. Grillo, R. Prohl, G. Wittum, A poroplastic model of structural reor-
978 ganisation in porous media of biomechanical interest, *Continuum Mech.*
979 *Therm.* 28 (2016) 579–601. doi:10.1007/s00161-015-0465-y.
- 980 [35] A. Grillo, R. Prohl, G. Wittum, A generalised algorithm for anelastic
981 processes in elastoplasticity and biomechanics, *Math. Mech. Solids* 22(3)
982 (2017) 502–527. doi:10.1177/1081286515598661.
- 983 [36] M. Mićunović, *Thermomechanics of Viscoplasticity*, Springer New York,
984 2009. doi:10.1007/978-0-387-89490-4.
- 985 [37] S. Sadik, A. Yavari, On the origins of the idea of the multiplicative
986 decomposition of the deformation gradient, *Mathematics and Mechanics*
987 *of Solids* 22 (4) (2017) 771–772. doi:10.1177/1081286515612280.
- 988 [38] E. Kröner, Allgemeine Kontinuumstheorie der Versetzungen und
989 Eigenspannungen, *Archive for Rational Mechanics and Analysis* 4 (1)
990 (1959) 273–334. doi:10.1007/bf00281393.

- 991 [39] A. Klarbring, T. Olsson, J. Stålhand, Theory of residual stresses with
992 application to an arterial geometry, *Arch. Mech.* 59(4–5) (2007) 341–364.
- 993 [40] A. Yavari, A geometric theory of growth mechanics, *J. Nonlinear Sci.* 20
994 (2010) 781–830. doi:10.1007/s00332-010-9073-y.
- 995 [41] A. Yavari, A. Goriely, Weyl geometry and the nonlinear mechanics of
996 distributed point defects, *Proc. R. Soc. A* 468 (2012) 3902–3922. doi:
997 10.1098/rspa.2012.0342.
- 998 [42] M. Epstein, Self-driven continuous dislocations and growth, in: M. G.
999 Steinmann P. (Ed.), *Mechanics of Material Forces. Advances in Mechan-*
1000 *ics and Mathematics*, Vol. 11, Springer, Boston, MA, 2005, pp. 129–139.
1001 doi:10.1007/0-387-26261-x_13.
- 1002 [43] P. Ciarletta, D. Ambrosi, G. Maugin, Mass transport in morphogenetic
1003 processes: A second gradient theory for volumetric growth and material
1004 remodeling, *J. Mech. Phys. Solids* 60 (2012) 432–450. doi:10.1016/j.
1005 *jmps*.2011.11.011.
- 1006 [44] M. Minozzi, P. Nardinocchi, L. Teresi, V. Varano, Growth-induced
1007 compatible strains, *Math. Mech. Solids* 22 (1) (2016) 62–71. doi:
1008 10.1177/1081286515570510.
- 1009 [45] A. Goriely, *The Mathematics and Mechanics of Biological Growth*,
1010 Springer New York, 2016. doi:10.1007/978-0-387-87710-5.
- 1011 [46] P. Nardinocchi, L. Teresi, V. Varano, The elastic metric: A review of
1012 elasticity with large distortions, *Int. J. Nonlinear Mech.* 56 (2013) 34–42.
1013 doi:10.1016/j.ijnonlinmec.2013.05.002.
- 1014 [47] J. Lubliner, *Plasticity Theory*, Dover Publications, Inc., Mineola, New
1015 York, 2008.
- 1016 [48] M. Epstein, M. Elżanowski, *Material Inhomogeneities and their Evo-*
1017 *lution — A Geometric Approach*, 1st Edition, Springer-Verlag Berlin
1018 Heidelberg, 2007. doi:10.1007/978-3-540-72373-8.
- 1019 [49] M. Epstein, *The geometric language of continuum mechanics*, Cam-
1020 bridge University Press, 2010.
- 1021 [50] A. Menzel, Modelling of anisotropic growth in biological tissues — a new
1022 approach and computational aspects, *Biomechan. Model. Mechanobiol.*
1023 3 (2005) 147–171. doi:10.1007/s10237-004-0047-6.

- 1024 [51] T. Olsson, A. Klarbring, Residual stresses in soft tissue as a consequence
1025 of growth and remodeling: application to an arterial geometry, *Eur. J.*
1026 *Mech. A* 27(6) (2008) 959–974. doi:10.1016/j.euromechsol.2007.
1027 12.006.
- 1028 [52] C. Voutouri, F. Mpekris, P. Papageorgis, A. D. Odysseos,
1029 T. Stylianopoulos, Role of constitutive behavior and tumor-host me-
1030 chanical interactions in the state of stress and growth of solid tu-
1031 mors, *PLoS ONE* 9 (8) (2014) e104717. doi:10.1371/journal.pone.
1032 0104717.
- 1033 [53] F. Mpekris, S. Angeli, A. P. Pirentis, T. Stylianopoulos, Stress-
1034 mediated progression of solid tumors: effect of mechanical stress
1035 on tissue oxygenation, cancer cell proliferation, and drug delivery,
1036 *Biomech. Model. Mechanobiol.* 14 (6) (2015) 1391–1402. doi:10.1007/
1037 s10237-015-0682-0.
- 1038 [54] P. Mascheroni, M. Carfagna, A. Grillo, D. Boso, B. Schrefler, An avascu-
1039 lar tumor growth model based on porous media mechanics and evolving
1040 natural states, *Mathematics and Mechanics of Solids* 23 (4) (2018) 686–
1041 712. doi:10.1177/1081286517711217.
- 1042 [55] D. Ambrosi, L. Preziosi, On the closure of mass balance models for
1043 tumor growth, *Mathematical Models and Methods in Applied Sciences*
1044 12 (05) (2002) 737–754. doi:10.1142/s0218202502001878.
- 1045 [56] D. Ambrosi, F. Mollica, The role of stress in the growth of a mul-
1046 ticell spheroid, *J. Math. Biol.* 49 (2004) 477–499. doi:10.1007/
1047 s00285-003-0238-2.
- 1048 [57] C. Giverso, M. Scianna, A. Grillo, Growing avascular tumours as elasto-
1049 plastic bodies by the theory of evolving natural configurations, *Mech.*
1050 *Res. Commun.* 68 (2015) 31–39. doi:http://dx.doi.org/10.1016/j.
1051 mechrescom.2015.04.004.
- 1052 [58] G. Helmlinger, P. A. Netti, H. C. Lichtenbeld, R. J. Melder, R. K. Jain,
1053 Solid stress inhibits the growth of multicellular tumor spheroids, *Nature*
1054 *Biotechnology* 15 (8) (1997) 778–783. doi:10.1038/nbt0897-778.
- 1055 [59] S. Preston, M. Elzanowski, Material uniformity and the concept of the
1056 stress space, in: B. Albers (Ed.), *Continuous Media with Microstructure*,
1057 1st Edition, Springer-Verlag Berlin Heidelberg, 2010, pp. 91–101. doi:
1058 10.1007/978-3-642-11445-8.

- 1059 [60] V. Ciancio, M. Dolfi, M. Francaviglia, S. Preston, Uniform materials
1060 and the multiplicative decomposition of the deformation gradient in fi-
1061 nite elasto-plasticity, *J. Non-Equilib. Thermodyn.* 33(3) (2008) 199–234.
1062 doi:10.1515/JNETDY.2008.009.
- 1063 [61] J. Marsden, T. Hughes, *Mathematical Foundations of Elasticity*, Dover
1064 Publications, Inc., Mineola, New York, 1983.
- 1065 [62] L. S. Bennethum, M. A. Murad, J. H. Cushman, Macroscale ther-
1066 modynamics and the chemical potential for swelling porous media,
1067 *Transport in Porous Media* 39 (2) (2000) 187–225. doi:10.1023/a:
1068 1006661330427.
- 1069 [63] G. Sciarra, G. A. Maugin, K. Hutter, A variational approach to a micro-
1070 structured theory of solid-fluid mixtures, *Archive of Applied Mechanics*
1071 73 (2003) 194–224. doi:10.1007/s00419-003-0279-4.
- 1072 [64] R. Serpieri, F. Travascio, *Variational continuum multiphase poroelastic-*
1073 *ity*, Springer Singapore, 2017. doi:10.1007/978-981-10-3452-7.
- 1074 [65] G. Ateshian, J. Weiss, Anisotropic hydraulic permeability under finite
1075 deformation, *J. Biomech. Engng.* 132 (2010) 111004–1–111004–7. doi:
1076 10.1115/1.4002588.
- 1077 [66] M. H. Holmes, V. C. Mow, The nonlinear characteristics of soft gels and
1078 hydrated connective tissues in ultrafiltration., *Journal of biomechanics*
1079 23 (1990) 1145–1156. doi:10.1016/0021-9290(90)90007-P.
- 1080 [67] S. Cleja-Tigoiu, G. A. Maugin, Eshelby’s stress tensors in finite elasto-
1081 plasticity, *Acta Mechanica* 139 (1-4) (2000) 231–249. doi:10.1007/
1082 bf01170191.
- 1083 [68] A. Tomic, A. Grillo, S. Federico, Poroelastic materials reinforced by
1084 statistically oriented fibres — numerical implementation and application
1085 to articular cartilage, *IMA J. Appl. Math.* 79 (2014) 1027–1059. doi:
1086 10.1093/imamat/hxu039.
- 1087 [69] A. Bazykin, *Nonlinear dynamics of interacting populations*, World Sci-
1088 entific Publishing, Singapore New Jersey London Hong Kong, 1998.
- 1089 [70] T. Stylianopoulos, J. D. Martin, M. Snuderl, F. Mpekris, S. R. Jain,
1090 R. K. Jain, Coevolution of solid stress and interstitial fluid pressure
1091 in tumors during progression: Implications for vascular collapse, *Cancer*
1092 *Research* 73 (13) (2013) 3833–3841. doi:10.1158/0008-5472.
1093 can-12-4521.

- 1094 [71] M. A. J. Chaplain, L. Graziano, L. Preziosi, Mathematical modelling
1095 of the loss of tissue compression responsiveness and its role in solid
1096 tumour development, *Mathematical Medicine and Biology: A Journal*
1097 of the IMA 23 (3) (2006) 197–229. doi:10.1093/imammb/dql009.
- 1098 [72] J. J. Casciari, S. V. Sotirchos, R. M. Sutherland, Mathematical mod-
1099 elling of microenvironment and growth in EMT6/ro multicellular tu-
1100 mour spheroids, *Cell Proliferation* 25 (1) (1992) 1–22. doi:10.1111/j.
1101 1365-2184.1992.tb01433.x.
- 1102 [73] J. J. Casciari, S. V. Sotirchos, R. M. Sutherland, Variations in tumor cell
1103 growth rates and metabolism with oxygen concentration, glucose con-
1104 centration, and extracellular pH, *Journal of Cellular Physiology* 151 (2)
1105 (1992) 386–394. doi:10.1002/jcp.1041510220.
- 1106 [74] P. Mascheroni, C. Stigliano, M. Carfagna, D. P. Boso, L. Preziosi,
1107 P. Decuzzi, B. A. Schrefler, Predicting the growth of glioblas-
1108 toma multiforme spheroids using a multiphase porous media model,
1109 *Biomech. Model. Mechanobiol.* 15 (5) (2016) 1215–1228. doi:10.1007/
1110 s10237-015-0755-0.